Journal of Catalysis 267 (2009) 140–157

Contents lists available at ScienceDirect

Journal of Catalysis

journal homepage: www.elsevier.com/locate/jcat

Mechanism of oxidations with H_2O_2 catalyzed by vanadate anion or oxovanadium(V) triethanolaminate (vanadatrane) in combination with pyrazine-2-carboxylic acid (PCA): Kinetic and DFT studies

Marina V. Kirillova [a], Maxim L. Kuznetsov [a], Vladimir B. Romakh [b], Lidia S. Shul'pina [c], João J.R. Fraústo da Silva [a], Armando J.L. Pombeiro [a,*], Georgiy B. Shul'pin [d,*]

[a] Centro de Química Estrutural, Complexo I, Instituto Superior Técnico, TU Lisbon, Av. Rovisco Pais, 1049-001 Lisbon, Portugal
[b] University of Western Ontario, Biological and Geological Sciences Building, London, Ontario, Canada N6A 5B7
[c] Nesmeyanov Institute of Organoelement Compounds, Russian Academy of Sciences, Ulitsa Vavilova, dom 28, Moscow 119991, Russia
[d] Semenov Institute of Chemical Physics, Russian Academy of Sciences, Ulitsa Kosygina, dom 4, Moscow 119991, Russia

ARTICLE INFO

Article history:
Received 19 June 2009
Revised 6 August 2009
Accepted 7 August 2009
Available online 11 September 2009

Keywords:
Alkane oxidation
Cyclohexane
Homogeneous catalysis
Hydrogen peroxide
Hydroxyl radical
Vanadium complexes

ABSTRACT

The oxovanadium(V) triethanolaminate complex (vanadatrane, **2**), in the presence of pyrazine-2-carboxylic acid (PCA) and H_2O_2, is shown to act as a catalyst for the efficient oxidation of isopropanol to acetone (without other solvents) and of cyclohexane (in MeCN) to cyclohexyl hydroperoxide at low temperature (40–50 °C). This catalytic system, that is similar to the previously discovered "vanadate ion (**1**)–PCA–H_2O_2" reagent, is investigated by detailed spectroscopic, kinetic, and DFT methods which allow us to establish the mechanism of the oxidations. The kinetic and spectroscopic studies reveal that both catalytic systems activate C–H bonds *via* a common reaction mechanism. The ^{51}V NMR data show that catalytic cycles involve the same intermediate species. Calculations by the DFT method allow us to explore intimate details of the mechanism of free radical generation and to introduce modifications to the mechanistic proposals published previously. Thus, a "water-assisted" mechanism of H-transfer steps is suggested and shown to be more effective than the "PCA-assisted" or "robot's arm" mechanism. The formation of both HOO· and HO· radicals is more favorable along the cycle based on complexes containing only one peroxo fragment V(OO) ("cycle I") than in the cycle based on diperoxo species containing $V(OO)_2$ fragments ("cycle III"). The generation of the reactive HO· radicals occurs *via* the addition of H_2O_2 to the V^{IV} complex [V(OO)(OH)(pca)] (pca = anionic basic form of PCA) to produce [V^{IV}(OO)(OH)(pca)(H_2O_2)], followed by water-assisted H-transfer to the HO-ligand (the rate-limiting stage of the overall process), isomerization, and O–OH bond cleavage. The pca ligand is found to play a key role as a stabilizer of the transition state for the H-transfer.

1. Introduction

Vanadium derivatives play an important role in living nature [1–11] (see, particularly, recent books and reviews [1,2,8,9]). Thus, vanadium ions can play a role in biology as counterions for protein, DNA, RNA, and in various biological organelles [2]. The vanadium ion is an enzyme cofactor, and is found in certain tunicates and possibly mammals [2]. The insulin-like action of vanadium complexes is well known: a variety of such complexes lower elevated glucose levels in diabetic animals [2]. Vanadium derivatives catalyze various oxidation processes *in vitro* [12–22]. For example, vanadium pentoxide catalyzes the two-electron oxidation of Br^- to Br^+, using aqueous hydrogen peroxide under dilute acidic conditions, and vanadium-catalyzed oxidative bromination by means of dilute mineral acids, hydrogen peroxide, and alkali bromides is an effective method for the bromination of aromatic substrates [14]. Many papers have been devoted to vanadium-catalyzed oxidation of hydrocarbons [23–63], particularly, alkanes [23–32,42,47], benzene [33,44,60], aromatic hydrocarbons [48,63], and olefins [43].

Earlier it has been found that the vanadate anion, VO_3^-, efficiently catalyzes the oxidation of organic compounds with H_2O_2 in acetonitrile, if pyrazine-2-carboxylic acid (PCA) is present as a co-catalyst in the solution in low concentrations [64–92]. The optimal ratio PCA/vanadate has been found to be 4:1 or 5:1, and the typical concentration of the vanadate anion was 0.1 mM. The oxidation of alkanes has been studied in more detail [64–73,75,79–81,90] although oxidative functionalization of benzene [64,76,80], olefins [74] and alcohols [64,79,80] has also been

* Corresponding authors. Fax: +351 21 8464455 (A.J.L. Pombeiro); +7 495 9397417/6512191 (G.B. Shul'pin).
E-mail addresses: pombeiro@ist.utl.pt (A.J.L. Pombeiro), Shulpin@chph.ras.ru, gbsh@mail.ru (G.B. Shul'pin).

0021-9517/$ - see front matter © 2009 Elsevier Inc. All rights reserved.
doi:10.1016/j.jcat.2009.08.006

described. It has been demonstrated later that PCA also accelerates oxidations catalyzed by iron [93–96], rhenium [97–99], and manganese [100] derivatives. In the present paper, we use PCA to name pyrazine-2-carboxylic acid. In some cases to depict the acidic nature of this compound we use the formula pcaH, where pca^- is pyrazine-2-carboxylate and H^+ is the proton.

The catalytic cycle for vanadium-catalyzed oxidations involves the formation of hydroperoxyl ($HOO^{\cdot}$) and hydroxyl ($HO^{\cdot}$) radicals as well as peroxo complexes of V^V and V^{IV} (Scheme 1 and S1). The co-catalyst PCA has been assumed to accelerate the proton transfer from a coordinated hydrogen peroxide molecule to oxo or hydroxy or peroxo ligands in the coordination sphere of vanadium complex ("robot's arm mechanism", Scheme 2) [75,79].

More recently, Bell and co-workers published density functional theory (DFT) calculation results concerning the oxidation mechanism by the H_2O_2–vanadate–PCA reagent [101]. The pca-ligand-assisted transfer of hydrogen atom ("robot's arm mechanism" proposed in [75]) was found to be more thermodynamically favored than the direct proton transfer to the vanadium-oxo group (steps *a* and *c* in Scheme 1) and occurs *via* migration of proton from a coordinated H_2O_2 molecule to the oxygen of a pca-ligand connected to the vanadium center (Scheme 2). Furthermore, the activation energy of the $HOO^{\cdot}$ radical generation (the rate-determining step *b*, Scheme 1) is substantially decreased, if a sequence of additional steps *via* diperoxo complexes is involved. Otherwise, the activation barrier for the V–OOH bond cleavage would be too high. Finally, it was demonstrated that the solvent coordination to vanadium complexes can play a significant role in this system. However, in another alkane oxidation system, based on the methyltrioxorhenium complex [$MeReO_3$], without PCA, it was very recently shown [102] that water could play an important role as a proton-transfer promoter, thus replacing PCA for such a purpose, although with a different pathway.

Continuing systematic studies on oxidations with H_2O_2 catalyzed by vanadate anion (**1**) we decided to investigate the possibility to use oxovanadium(V) triethanolaminate (vanadatrane, **2**) [103–107] containing a chelating ligand as a pre-catalyst and to compare the reactions catalyzed by **1**–PCA and **2**–PCA. Complex **2** was chosen as a possible pre-catalyst for this system in view of its known [28,38,50,52,56,107] catalytic activity for functionalization reactions of alkanes under mild conditions.

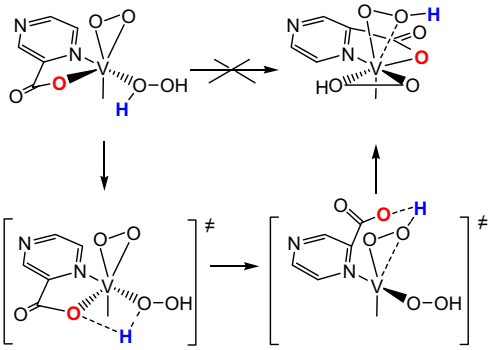

Scheme 2. The "robot's arm mechanism" for the proton transfer from coordinated H_2O_2 molecule to the peroxo ligand [75,79].

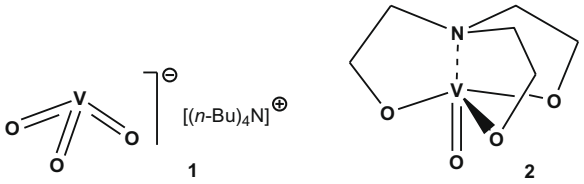

Here we describe a new common mechanistic scheme for oxidations with hydrogen peroxide, based on the **1**–PCA and **2**–PCA systems. Detailed insights into the catalytic cycle of radical generation are disclosed using kinetic data and quantum chemical calculations at the DFT level of theory. In particular, the search for more favorable mechanisms than those previously proposed and the establishment of the roles of PCA and water constitute the important aims of the current study.

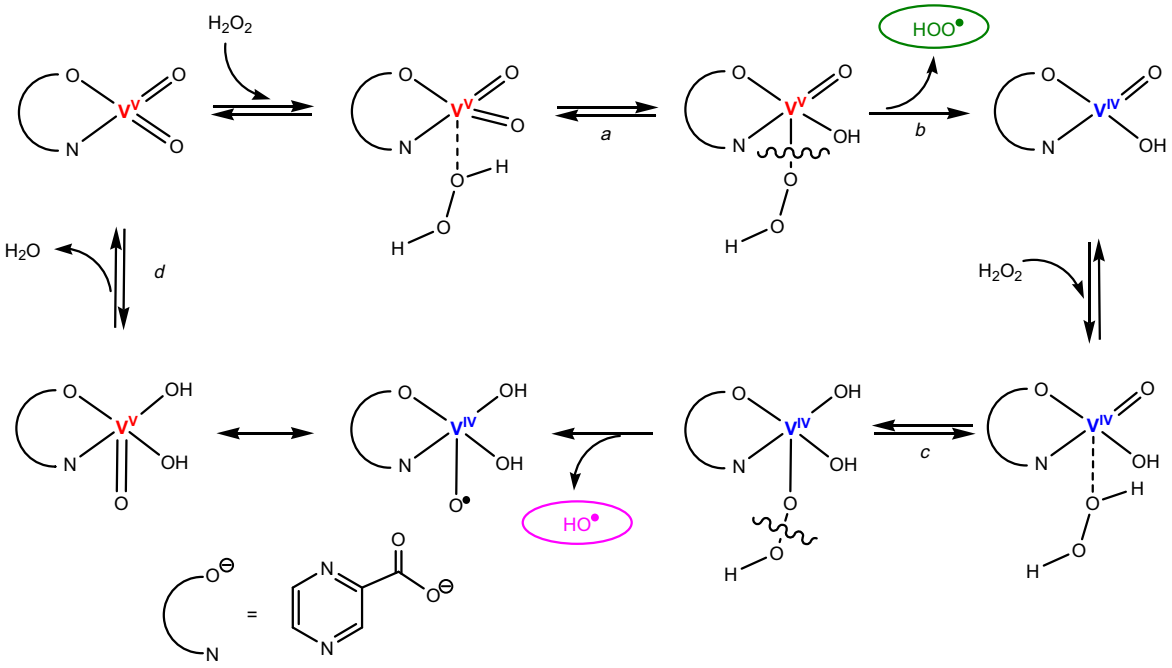

Scheme 1. Proposed [75,79] catalytic cycle for hydroperoxyl and hydroxyl radicals generation catalyzed by the vanadate–PCA system.

2. Experimental

2.1. Oxidation experiments

Catalysts **1** [75] and **2** [103–107] and co-catalyst PCA were used in the form of stock solutions in isopropanol or acetonitrile. Aliquots of these solutions were added to the reaction mixtures in the oxidations of isopropanol or alkanes. The oxidation reactions were typically carried out in air in thermostated (40 or 50 °C in the case of cyclohexane or isopropanol oxidation, respectively) Pyrex cylindrical vessels with vigorous stirring (**CAUTION**: the combination of air or molecular oxygen and H_2O_2 with organic compounds at elevated temperatures may be explosive!). The reactions were stopped by cooling, and were analyzed twice, *i.e.*, before and after the addition of an excess of solid PPh_3. This method was developed and used previously by some of us [30,31,63] for the analysis of reaction mixtures obtained from various alkane oxidations. Applying this method in the present work for the oxidation of cyclohexane, we demonstrate that the reaction affords predominantly the cyclohexyl hydroperoxide as a primary product which slowly decomposes to form cyclohexanol and cyclohexanone. In our kinetic studies for precise determination of oxygenate concentrations only data obtained after reduction of the reaction sample with PPh_3 were used. A Fisons Instruments GC 8000 series gas chromatograph with a capillary column 30 m × 0.32 mm × 25 μm, DB-WAX (J&W) (helium was the carrier gas; the internal standard was nitromethane) was used.

^{1}H and ^{51}V NMR spectra were measured on a Bruker 400 UltraShield spectrometer at ambient temperature (297 K) in the presence of acetone-d_6 (1/5 vol) for magnetic field lock. The vanadium chemical shifts are quoted relative to external $VOCl_3$. A typical vanadium spectrum for a 1 mM solution was obtained from the accumulation of 20,000 transients with a 900 ppm spectral window, at about 10 scans per second. An exponential line broadening up to 200 Hz was applied before Fourier transformation. The UV–vis spectra were recorded on a Jasco model 7800 UV–vis spectrophotometer.

2.2. Computational details

The full geometry optimization of all structures and transition states has been carried out at the DFT level of theory using Becke's three-parameter hybrid exchange functional in combination with the gradient-corrected correlation functional of Lee, Yang and Parr (B3LYP) [108,109] with the help of the Gaussian-98 [110] program package. The restricted approximations for the structures with closed electron shells and the unrestricted methods for the structures with open electron shells have been employed. Symmetry operations were not applied for all structures. The geometry optimization was carried out using a relativistic Stuttgart pseudopotential that described 10 core electrons and the appropriate contracted basis set (8s7p6d1f)/[6s5p3d1f] [111] for the vanadium atom and the 6-31G(d) basis set for other atoms. Then, for the species involving into the discussed mechanisms, single-point calculations were performed on the basis of the found equilibrium geometries using the 6-31+G(d,p) basis set for non-metal atoms. The B3LYP functional in conjunction with Stuttgart pseudopotentials and the 6-31+G(d,p) basis set is a quite reasonable approach for the investigation of the reactivity and mechanism of reactions involving transition metal complexes, taking into account the low computational cost of this method and usual good agreement with the experimental data.

The Hessian matrix was calculated analytically for the optimized structures at the B3LYP/6-31G(d) level in order to prove the location of correct minima (no "imaginary" frequencies) or saddle points (only one negative eigenvalue), and to estimate the thermodynamic parameters, the latter being calculated at 25 °C. The nature of all transition states was investigated by the analysis of vectors associated with the "imaginary" frequency.

Total energies corrected for solvent effects (E_s) were estimated at the single-point calculations on the basis of gas-phase geometries using the conductor-like polarized continuum model (CPCM) [112,113] at the CPCM-B3LYP/6-31+G(d,p)//gas-B3LYP/6-31G(d) level of theory with CH_3CN and 2-propanol as solvents. The latter solvent was approximated by the values of the dielectric constant and solvent radius of 19.9 and 2.18 Å, respectively. The Gaussian-03 program package [114] was used for the calculations of the solvent effects and the united atom topological model was applied for the molecular cavity. The entropic term in CH_3CN solution (S_s) was calculated according to the procedure described by Wertz [115] and Cooper and Ziegler [116] using Eqs. (E1)–(E4):

$$\Delta S_1 = R \ln V^s_{m,liq}/V_{m,gas} \quad \text{(E1)}$$

$$\Delta S_2 = R \ln V^\circ_m/V^s_{m,liq} \quad \text{(E2)}$$

$$\alpha = \frac{S^{\circ,s}_{liq} - \left(S^{\circ,s}_{gas} + R \ln V^s_{m,liq}/V_{m,gas}\right)}{\left(S^{\circ,s}_{gas} + R \ln V^s_{m,liq}/V_{m,gas}\right)} \quad \text{(E3)}$$

$$\begin{aligned} S_s &= S_g + \Delta S_{sol} = S_g + [\Delta S_1 + \alpha(S_g + \Delta S_1) + \Delta S_2] \\ &= S_g + [(-12.21 \text{ cal/mol K}) - 0.23(S_g - 12.21 \text{ cal/mol K}) \\ &\quad + 5.87 \text{ cal/mol K}] \end{aligned} \quad \text{(E4)}$$

where S_g is the gas-phase entropy of solute, ΔS_{sol} the solvation entropy, $S^{\circ,s}_{liq}$, $S^{\circ,s}_{gas}$, and $V^s_{m,liq}$ are standard entropies and molar volume of the solvent in liquid or gas phases (149.62 and 245.48 J/mol K and 52.16 mL/mol, respectively, for CH_3CN), $V_{m,gas}$ is molar volume of the ideal gas at 25 °C (24450 mL/mol), and V°_m is molar volume of the solution corresponding to the standard conditions (1000 mL/mol). The enthalpies and Gibbs free energies in solution (H_s and G_s) were estimated using expressions (E5) and (E6)

$$H_s = E_s(\text{6-31+G(d,p)}) + H_g(\text{6-31G(d)}) - E_g(\text{6-31G(d)}) \quad \text{(E5)}$$

$$G_s = H_s - TS_s \quad \text{(E6)}$$

where E_s, E_g, and H_g are the total energies in solution and in gas phase and gas-phase enthalpy calculated at the corresponding level.

3. Results and discussion

3.1. NMR spectra of the vanadatrane (2)–PCA–H_2O_2 combination

^{51}V NMR spectroscopy was found to be a powerful tool in the identification of vanadium species under reaction conditions in both acetonitrile [75] and isopropanol [79]. An isopropanol solution with a constant water concentration (2.2 M) was used. The ^{51}V NMR spectrum of a 1 mM vanadatrane (**2**) solution is shown in Fig. 1, *Graph A*, spectrum a. The spectrum consists of three resonances at −384 ppm (signal A, **2**), −448 ppm (C), and a major one at −631 ppm (B), which corresponds to compound $[VO(O\text{-}i\text{-}Pr)_3]$ (**3**; Scheme 3) according to the literature data [117,118]. Thus, **3** is more easily formed from **2** than from **1** in *i*-PrOH [117–119], where an addition of trifluoroacetic acid is needed. In the presence of 4-fold excess of PCA, signal A from **2** almost disappears while signal B is still present along with a new broad one at −545 ppm (D, Fig. 1c). Exactly the same pattern we observed previously [79] for **1** under these conditions (see Fig. 1, *Graph B* for comparison), signal D being attributed to $[VO_2(pca)_2]^-$ (**4**). Clearly, PCA facilitates the formation of **3** from **2** in *i*-PrOH.

Addition of H_2O_2 results in dramatic changes in ^{51}V NMR spectra. Both signals B and D vanish, while a new major resonance E ap-

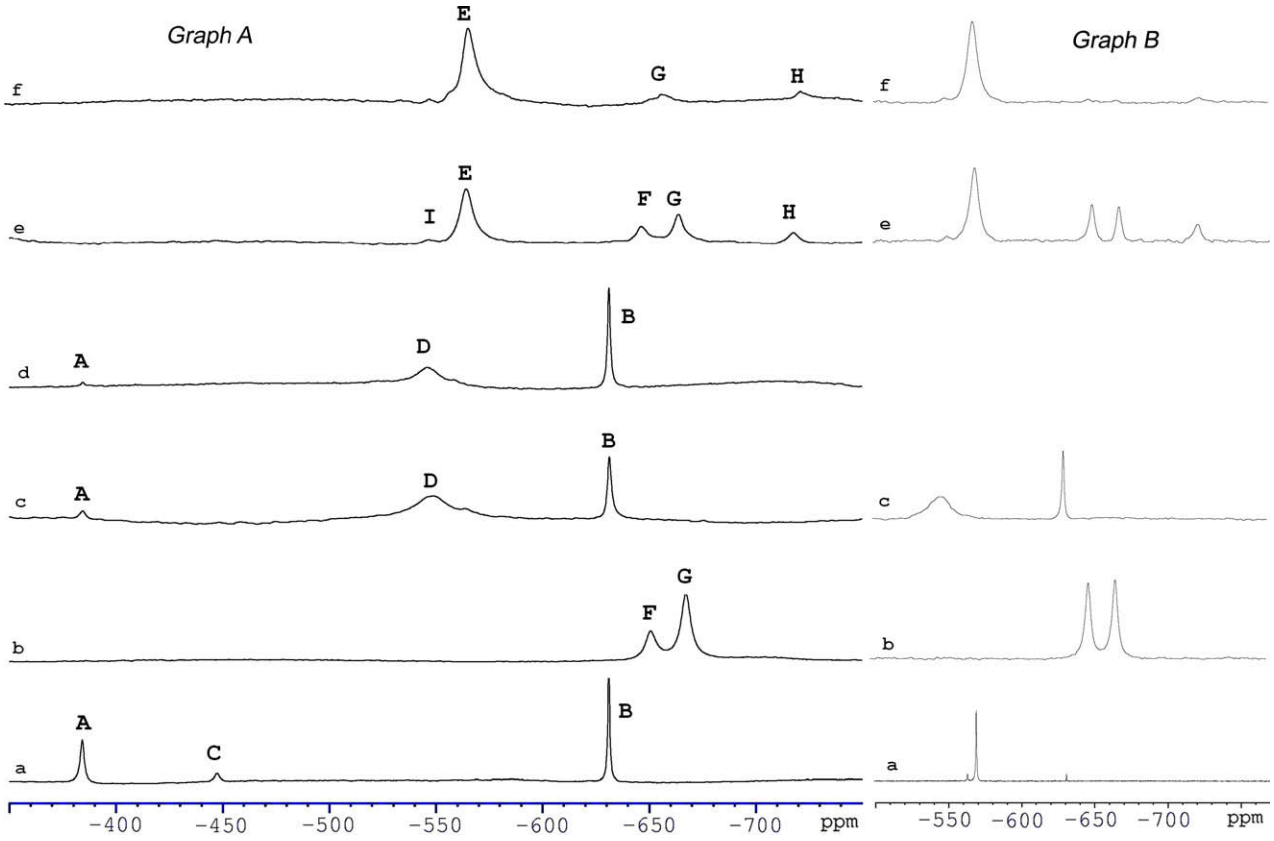

Fig. 1. *Graph A*: ^{51}V NMR spectra of (a) **2** (1 mM); (b) **2** (1 mM) + H_2O_2 (0.5 M); (c) **2** (1 mM) + PCA (4 mM); (d) **2** (1 mM) + PCA (10 mM); (e) **2** (1 mM) + PCA (4 mM) + H_2O_2 (0.5 M); (f) **2** (1 mM) + PCA (10 mM) + H_2O_2 (0.5 M). *Graph B* (adapted from [79]): ^{51}V NMR spectra of the same solutions but with compound **1** instead of **2** (spectrum f: [PCA] = 12 mM). All spectra were recorded in isopropanol containing 2.2 M H_2O.

pears (δ −565 ppm) (Fig. 1e) as well as three new vanadium resonances of comparable intensities in the high field region, typical for diperoxo complexes: δ −647 (F), −664 (G), and −719 (H). All these new signals are identical to those observed for the **1**–PCA system [75,79]. Thus, under catalytic conditions the major vanadium species is complex **5** (signal E). Signal I at −550 ppm corresponds to its minor isomer **6** and signal H corresponds to a diperoxo species with the tentative $[VO(OO)(OOH)(pca)]^-$ (**7**) description. It turned out that the two low field signals (F and G) are formed also in the absence of PCA (Fig. 1b). Earlier [120–122] the upfield component was attributed to an aqua-diperoxovanadium species, while the downfield resonance was attributed to diperoxo species containing isopropanol molecule under comparable conditions. Thus, the same complexes can be responsible for signals G ($[VO(OO)_2(H_2O)]^-$, **8**) and F ($[VO(OO)_2(i\text{-PrOH})]^-$, **9a**) in the ^{51}V NMR spectra. Moreover, the relative intensity of signal G, corresponding to the aqua-diperoxo species, increases at higher water concentrations.

We recorded the same set of spectra for **2** using acetonitrile as a solvent with a fixed water concentration (2.2 M), and the results are shown in Fig. 2. Vanadatrane is stable in wet acetonitrile solution (signal A, Fig. 2a), but is transformed completely to diperoxo vanadium species in the presence of H_2O_2 (Fig. 2b). The relative intensity of signal G is very sensitive to water concentration and can be assigned to $[VO(OO)_2(H_2O)]^-$ (**8**). However, the resonance is shifted downfield (δ −644 vs. δ −664 ppm, isopropanol) due to the different compositions of the solvation shell in these two solvents. Signal J at δ −699 ppm can be attributed to $[VO(OO)_2(NCCH_3)]^-$ (**9b**) by analogy with species **9a**, as far as this signal appears only in the presence of acetonitrile.

The significant difference in the ^{51}V NMR line widths (2400 Hz in isopropanol vs. 450 Hz in acetonitrile) can be explained by the difference in the solution viscosities. The NMR line width of vanadium-51 is controlled by quadrupolar relaxation, and it is proportional to the rotational correlation time τ_c, which in turn is proportional to the viscosity. The ratio of the line widths for D in isopropanol and for $[VO_2(pca)_2]^-$ in acetonitrile is roughly the same as the ratio of viscosities of isopropanol and acetonitrile at room temperature (2.04 and 0.34 mPa s, respectively) [123]. In mixed acetonitrile–isopropanol solvents of different compositions, we observed gradual changes in vanadium NMR spectra on transition from pure acetonitrile to pure isopropanol. The signal from $[VO_2(pca)_2]^-$ broadened, and the concentration of $[VO(O\text{-}i\text{-}Pr)_3]$ increased with increasing the relative content of isopropanol (Fig. 6 [79]). The vanadium spectra obtained in binary solvents contained no new, previously undetected resonances.

Visually, the signal from $[VO(O\text{-}i\text{-}Pr)_3]$ (B) in Fig. 1 seems broader in the presence of PCA than in its absence (spectra 1a, 1c and 1d). On the first glance, this could be interpreted as an indication of some structural changes generated by PCA for this complex. However, this effect is only apparent and it results from exponential multiplication with a strong line broadening (200 Hz) applied for reliable detection of the very broad signal D. When we process spectra 1a and 1c with the same line broadening, the line widths of signal B in these spectra are identical.

Species $[VO_2(pca)_2]^-$ (**4**) is formed in the presence of PCA from **2** in both acetonitrile and isopropanol: signal D is shifted downfield to δ −536 ppm in acetonitrile solution (Fig. 2c and d). However, when H_2O_2 is then added to the acetonitrile solution, monoperoxo vanadium complexes **5** and **6** are formed preferentially rather than

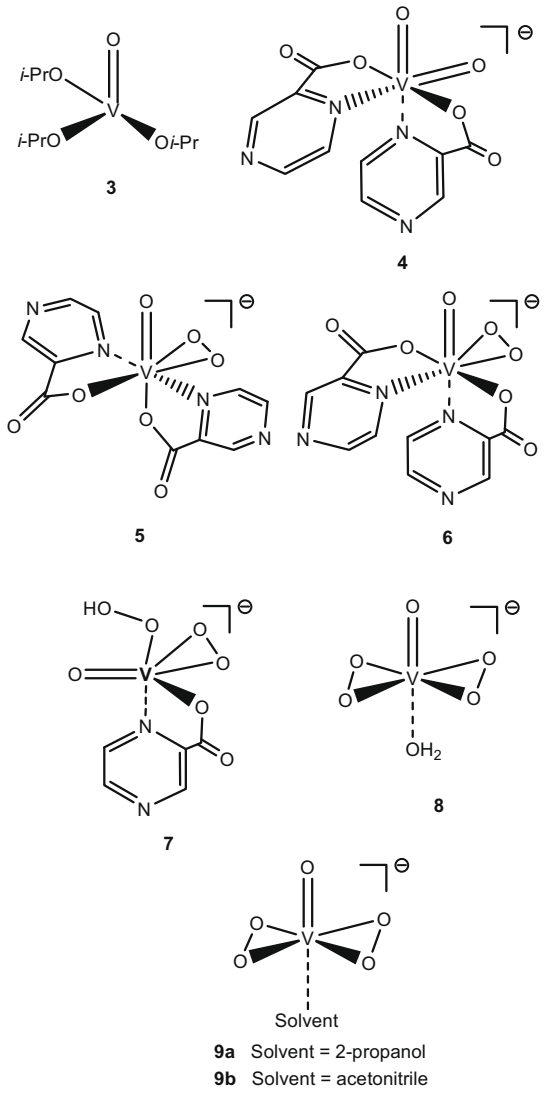

Scheme 3. Vanadium-containing species detected by ^{51}V NMR in the oxidation of isopropanol with H_2O_2, catalyzed by the **1**–PCA and **2**–PCA systems.

diperoxo species in analogous conditions in isopropanol. Apparently, the proton transfer to coordinated pca-ligand in **5** and **6** is facilitated in the more polar isopropanol than in acetonitrile. As a result, the protonated pcaH-ligand can be replaced by hydrogen peroxide to form a diperoxo vanadium species. The results of ^{51}V NMR studies are summarized in Scheme 3 and Table 1.

The proton NMR spectrum of a mixture containing 4 mM **2**, 16 mM PCA, and 4 mM H_2O_2 in isopropanol/water (Fig. 3a) shows three signals from free PCA (9.24, 8.85, and 8.80 ppm) in the aromatic region as well as six signals from monoperoxo vanadium complex **5** (9.92, 9.46, 9.41, 9.39, 9.37, and 9.23 ppm), where two pca-ligands are not equivalent. However, in acetonitrile solution the same mixture gave three additional signals (Fig. 3b, marked with #) with δ 9.22, 8.77, and 8.45 due to the presence of **4**, containing no peroxo ligands. The equilibrium between **4** and **5** under these conditions has also been established by ^{51}V NMR. Thus, in acetonitrile solution, **4** is only partially converted to **5**, and the replacement (following step) of a pca-ligand in the latter complex by hydrogen peroxide is retarded, in comparison with the more polar isopropanol. The difference in proton chemical shifts of the pca ligands in acetonitrile and in isopropanol is too subtle, however, to consider them as strong evidence for entering isopropanol into the first coordination sphere of vanadium for these oxo–peroxo complexes. The same pattern was observed in ^{1}H NMR for the **1**–PCA system in acetonitrile and isopropanol [75,79] which allows us to conclude that we deal with the same vanadium species.

Finally, common-type vanadium-containing species are detectable for **1** and **2** in acetonitrile and isopropanol under the catalytic conditions (Scheme 3): two isomers of the monoperoxo vanadium complex $[VO(OO)(pca)_2]^-$ (**5**, **6**) and the diperoxo species $[VO(OO)_2(H_2O)]^-$ (**8**) as well as $[VO(OO)_2(Solvent)]^-$ (**9a**, **9b**). The diperoxo intermediate with a tentative description $[VO(OO)(OOH)(pca)]^-$ (**7**) was observed only in isopropanol. The monoperoxo–diperoxo conversion is less efficient at higher PCA concentrations. It is reasonable to assume that PCA competes with H_2O_2 for coordination sites and, at high concentrations, stabilizes monoperoxo complexes $[VO(OO)(pca)_2]^-$, whereas the formation of the diperoxo species, being the plausible catalytically active form according to the previous DFT calculations [101], is suppressed. Obviously, there should be an "optimal" PCA concentration, at which the degree of such monoperoxo–diperoxo conversion reaches the maximum.

3.2. Electronic spectra of the vanadatrane–PCA–H_2O_2 combination

The NMR data indicate that catalytically active peroxovanadium complexes containing pca-ligands species are produced *via* the same mechanism for both **1** and **2**. We also studied the reaction mixtures by UV–vis spectroscopy and found that the addition of PCA to a **1** or **2** (10^{-3} M) solution containing H_2O_2 leads to the appearance of a new absorption band in the visible region with maximum at 457 nm. Previously it was shown [79] that this is due to the formation of the monoperoxo vanadium species **5** with molar extinction coefficient $\varepsilon_{457} = 350 \pm 10\ M^{-1}\ cm^{-1}$. Indeed, this absorption does not exist in the absence of either H_2O_2 or PCA. Moreover, PCA, H_2O_2 as well as the complexes **8** and **9a** have no absorption in this region.

In acetonitrile and isopropanol, the stereoisomer **5** is the predominant species in solution under the catalytic conditions. Starting from **1**, it can be isolated in almost quantitative yield and the X-ray structure is available [84]. While in acetonitrile **5** is pretty stable even at high concentrations of H_2O_2, in isopropanol a series of diperoxo species **7**, **8**, and **9a** is formed according to the ^{51}V NMR studies. The UV–vis spectra changes are shown in Fig. 4. With a 4-fold excess of H_2O_2 over the vanadatrane (**2**) concentration (Fig. 4, curve *1*), almost complete transformation into vanadium monoperoxo derivative **5** is observed. Indeed, the value of optical density D_{457} reaches its maximum and ^{51}V NMR spectra show the corresponding changes. However, upon further addition of H_2O_2 the absorbance at 457 nm decreases, the competition between H_2O_2 and PCA in the vanadium coordination sphere leads to diperoxo complexes formation. This transformation is readily achieved in isopropanol (Fig. 4A), while in acetonitrile higher concentrations of H_2O_2 are needed (Fig. 4B). Apparently, the protonation of anionic pca-ligand prior to displacement with H_2O_2 is more efficient in isopropanol than in acetonitrile. Such a displacement is retarded at higher concentration of PCA added to the reaction mixture (Fig. 5).

When hydrogen peroxide is added in a higher concentration (0.02–0.5 M, Fig. 4B), the concentration of **5** decreases, giving rise to the formation of diperoxo vanadium complexes. In moist isopropanol this transformation leads to complexes **7**, **8**, and **9a**. Both **8** and **9a**, containing no pca-ligand in the coordination sphere of vanadium, can be prepared in the absence of PCA and have no absorbance at 457 nm. We can show that ε_{457} of the diperoxo complex **7**, which cannot be prepared independently, is substantially smaller than that for **5**. At 0.5 M H_2O_2 the equilibrium distribution of these complexes can be estimated from ^{51}V NMR spectrum

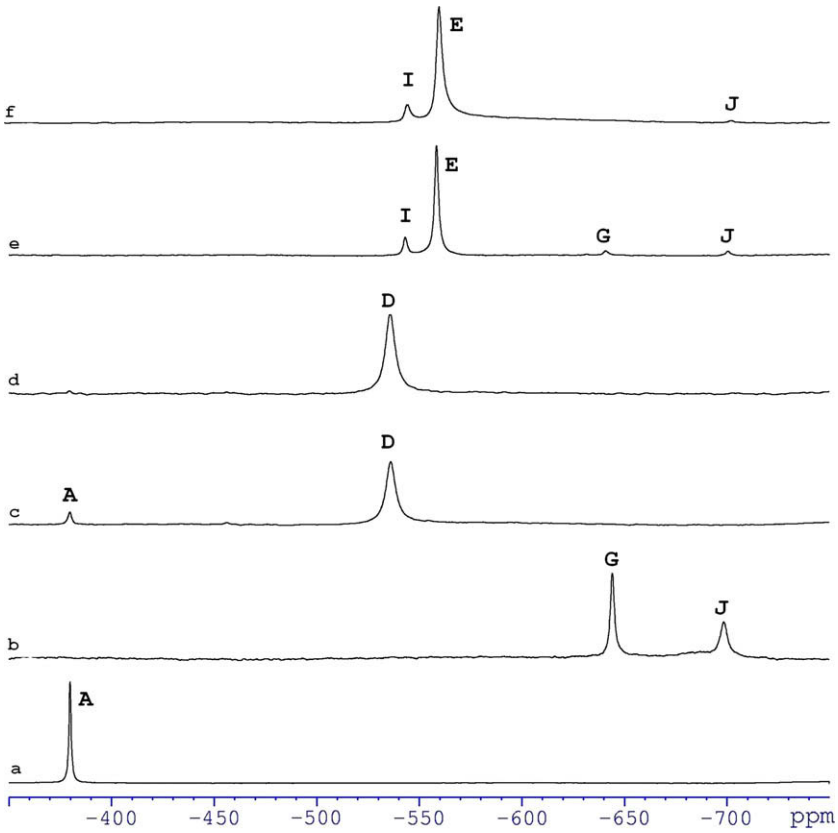

Fig. 2. ^{51}V NMR spectra of (a) **2** (1 mM); (b) **2** (1 mM) + H_2O_2 (0.5 M); (c) **2** (1 mM) + PCA (4 mM); (d) **2** (1 mM) + PCA (10 mM); (e) **2** (1 mM) + PCA (4 mM) + H_2O_2 (0.5 M); (f) **2** (1 mM) + PCA (10 mM) + H_2O_2 (0.5 M). All spectra were recorded in acetonitrile containing 2.2 M H_2O.

Table 1
^{51}V NMR shifts (δ, ppm) for vanadium species formed from complexes **1** (see [79]) and **2** in isopropanol and acetonitrile [δ ($VOCl_3$) = 0 ppm].

Species	In isopropanol	In acetonitrile
n-Bu_4NVO_3 (**1**)	–	−539
[$VO(O_3C_6H_{12}N)$] (**2**)	−384	−380
[VO(O-*i*-Pr)$_3$] (**3**)	−631	–
[$VO_2(pca)_2$]$^-$ (**4**)	−545	−536
cis-[V(O)(OO)$(pca)_2$]$^-$ (**5**)	−565	−558
trans-[V(O)(OO)$(pca)_2$]$^-$ (**6**)	−550	−543
[V(OO)(OOH)(pca)]$^-$ (**7**)	−719	–
[$VO(OO)_2(H_2O)$]$^-$ (**8**)	−664	−644
[$VO(OO)_2$(*i*-PrOH)] (**9a**)	−647	–
[$VO(OO)_2(NCCH_3)$]$^-$ (**9b**)	–	−699

shown in Fig. 1e [79]. Thus, [**5**] = 0.54 mM and the corresponding D_{457}(**5**) give a theoretical value 0.189 ± 0.006. The experimental D_{457} value is 0.187 for the whole mixture and was obtained in the presence of $[\mathbf{7}]_{1e}$ = 0.062 mM. Apparently, ε_{457}(**7**) is close to zero and complex **7** has an absorption maximum in a short-wave region of the spectrum (see Fig. 4A). Indeed, the diperoxovanadate species would have a blue-shifted charge transfer transition. In the case of **1**, the same approach gave $\varepsilon_{457}(\mathbf{7}) < 20\ M^{-1}\ cm^{-1}$. Thus, the absorbance at 457 nm is almost exclusively due to the presence of **5** in solution. Finally, the transformation of monoperoxo to diperoxo derivatives (Fig. 4) occurs to high extent, if the concentration of PCA is low, and even if hydrogen peroxide is added. These results testify that PCA and H_2O_2 compete for a site in the coordination sphere of vanadium. For both **1** and **2**, the changes in UV–vis spectra under the catalytic conditions are the same.

3.3. Oxidation of isopropanol

Isopropanol is easily oxidized by hydrogen peroxide in air to give acetone, if **1** or **2** is used in combination with PCA (Fig. 6). Otherwise, the catalytic reaction is very slow. In order to identify possible intermediates in the catalytic cycle, we performed detailed spectroscopic studies of the **2**–PCA system described in Sections 3.1 and 3.2. We compared our findings with the **1**–PCA combination, which was recently studied by ^{51}V NMR and UV–vis spectroscopy [79] and came to the conclusion that in the cases of both pre-catalysts **1** and **2** the same intermediate species are present in the reaction mixture.

We found that the oxidation activity of both systems is significantly suppressed at high water contents (Fig. 7), thus, in all experiments we fixed the concentration of water to 2.2 M. The yield of acetone is significantly lower, if the reaction is carried out in an argon atmosphere. This testifies that atmospheric oxygen takes part in the oxidation. However, the initial rates of the reaction in argon and in air are the same. Thus, in all further kinetic experiments only initial rates of the oxidation can be used.

We carried out a kinetic study of isopropanol oxidation catalyzed by **1** and **2** in the presence of PCA as a co-catalyst. The obtained results are shown in Figs. 6–11. A kinetic study was performed for **1** and **2** in moist isopropanol solutions, using hydrogen peroxide as a promoter. The dependences of initial rate W_0 of acetone accumulation on initial concentrations of pre-catalyst **1** or **2**, co-catalyst PCA and hydrogen peroxide are presented in Figs. 8–10.

The kinetic data demonstrate that the rate of isopropanol oxidation is directly proportional to the vanadium precursor concentration, regardless of the nature of starting compound. This fact is in

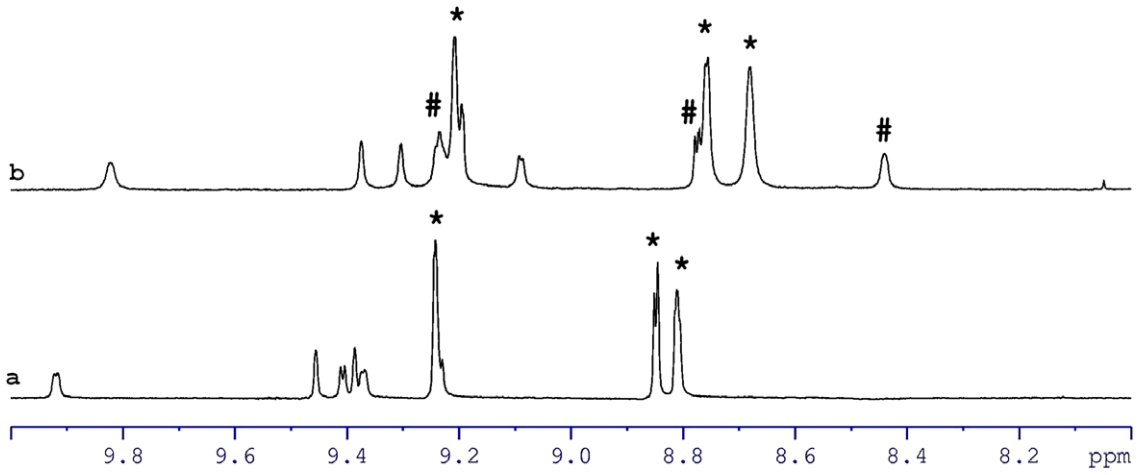

Fig. 3. ^{1}H NMR spectra of **2** (4 mM) + PCA (16 mM) + H_2O_2 (4 mM) in isopropanol; (b) acetonitrile. Peaks indicated by (*) and (#) are due to free PCA and **4**, respectively. Total water concentration was 2.2 M.

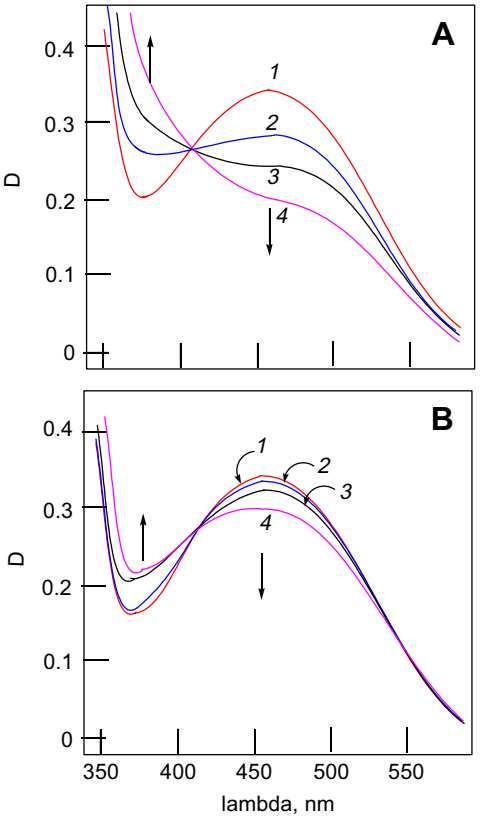

Fig. 4. Electronic spectra of **2** (1 mM) and PCA (4 mM) in isopropanol/water (2.2 M; Graph A) and acetonitrile/water (2.2 M; Graph B) solution at various concentrations of H_2O_2: 0.004 (1), 0.10 (2), 0.25 (3), 0.50 M (4); the components were mixed at 50 °C, 2 min before the spectra were recorded.

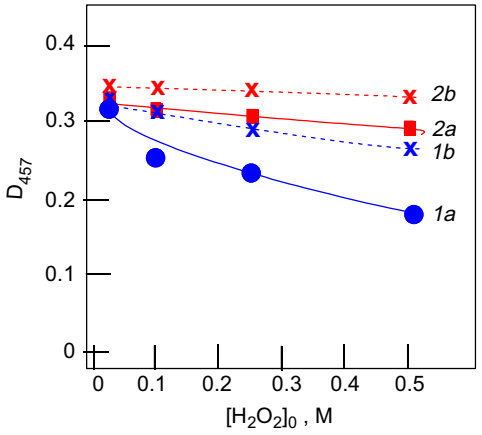

Fig. 5. Dependence of D_{457} on concentration of hydrogen peroxide in the electronic spectra of **2** (1 mM) solutions in isopropanol/water (2.2 M) (curves *1*) and in acetonitrile/water (2.2 M) (curves *2*) at two different concentrations of PCA: 0.004 (*a*), 0.010 M (*b*); the components were mixed at 50 °C, 2 min before the spectra were recorded.

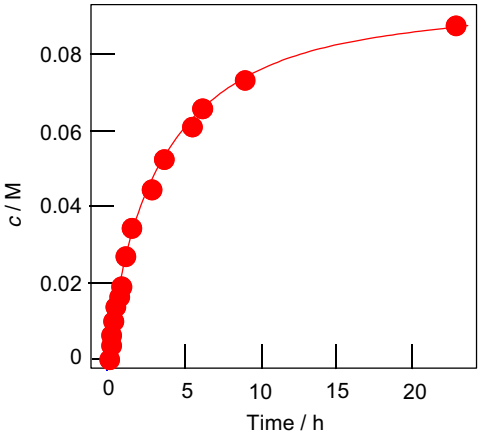

Fig. 6. Kinetic curve of acetone accumulation in isopropanol oxidation without solvent. Conditions: [vanadatrane **2**] = 1 mM, [PCA] = 5 mM, $[H_2O_2]_0$ = 0.50 M, $[H_2O]_{total}$ = 2.2 M; 50 °C.

line with the monovanadate species being involved in the oxidation reaction. In the absence of PCA the initial rate W_0 is low, therefore the catalytic activity of the vanadium complexes **8** and **9a**, which do not contain a pca-ligand in the coordination sphere, is low. For both species **1** and **2** in the presence of PCA the concentrations of the monoperoxo vanadium species and the corresponding absorption at 457 nm attain maximum values (Fig. 4) at low H_2O_2 concentrations (0–0.02 M), but the reaction rate is still low (Fig. 10). An increase in the reaction rate upon further addition of H_2O_2 is accompanied by the transformation of the monoperoxo vanadium complex $[VO(OO)(pca)_2]^-$ (**5**), being the predominant

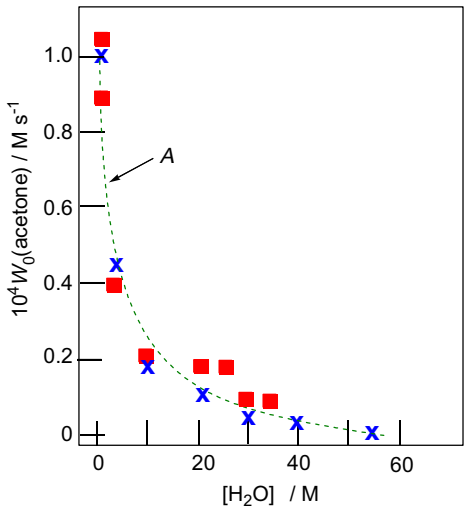

Fig. 7. Dependences of the initial rate of acetone accumulation in the isopropanol oxidation on water concentration. Blue crosses: [**1**] = 1 mM, [PCA] = 4 mM, $[H_2O_2]_0$ = 0.50 M, 50 °C. Red squares: [**2**] = 1 mM, [PCA] = 5 mM, $[H_2O_2]_0$ = 0.50 M; 50 °C. Dashed curve *A* is a theoretical curve calculated in accordance with the kinetic scheme described in Section 3.3. (For interpretation of the references to colour in this figure legend, the reader is referred to the web version of this article.)

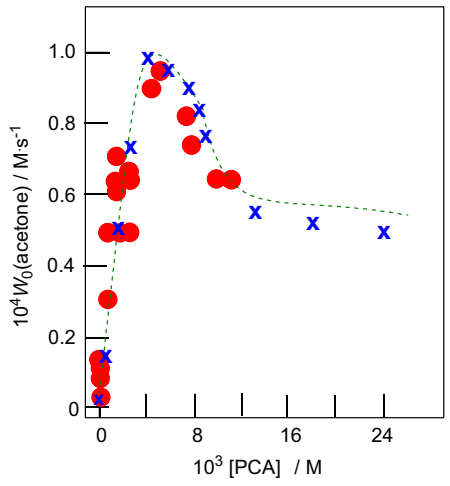

Fig. 9. Dependences of the initial rate W_0 of acetone accumulation in the isopropanol oxidation in isopropanol solution catalyzed by *n*-Bu_4NVO_3 (**1**) and vanadatrane (**2**) on the initial concentration of PCA. Blue crosses: [**1**] = 1 mM, [PCA] = 4 mM, $[H_2O_2]_0$ = 0.50 M, $[H_2O]$ = 2.2 M; 50 °C. Red circles: [**2**] = 1 mM, [PCA] = 5 mM, $[H_2O_2]_0$ = 0.50 M, $[H_2O]$ = 2.2 M; 50 °C. Dashed curve is a theoretical curve calculated in accordance with the kinetic scheme described in Section 3.3. (For interpretation of the references to colour in this figure legend, the reader is referred to the web version of this article.)

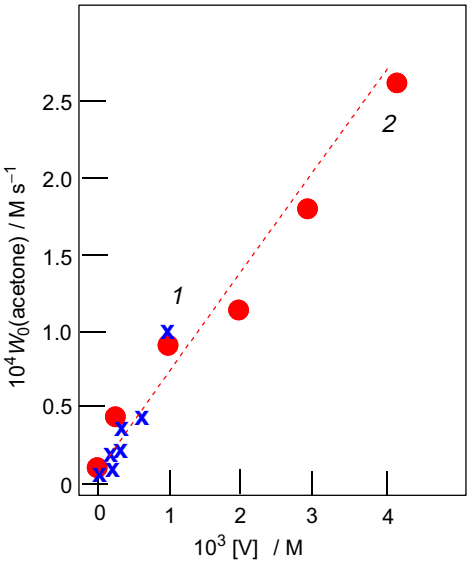

Fig. 8. Dependences of the initial rate W_0 of acetone accumulation in the isopropanol oxidation in isopropanol solution on the initial concentration of *n*-Bu_4NVO_3 (**1**) and vanadatrane (**2**). Blue crosses: [**1**] = 1 mM, [PCA] = 4 mM, $[H_2O_2]_0$ = 0.50 M, $[H_2O]$ = 2.2 M; 50 °C. Red circles: [**2**] = 1 mM, [PCA] = 5 mM, $[H_2O_2]_0$ = 0.50 M, $[H_2O]$ = 2.2 M; 50 °C. Dashed curve is a theoretical curve calculated in accordance with the kinetic scheme described in Section 3.3. (For interpretation of the references to colour in this figure legend, the reader is referred to the web version of this article.)

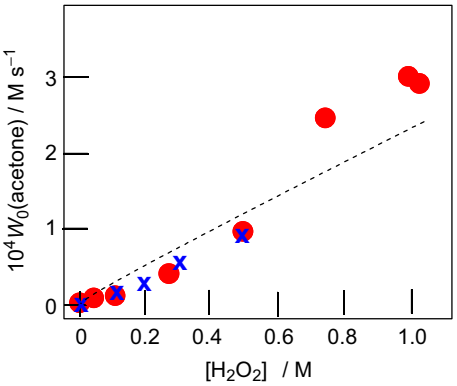

Fig. 10. Dependences of the initial rate W_0 of acetone accumulation in the isopropanol oxidation in isopropanol solution catalyzed by *n*-Bu_4NVO_3 (**1**) and vanadatrane (**2**) on the initial concentration of hydrogen peroxide. Blue crosses: [**1**] = 1 mM, [PCA] = 4 mM, $[H_2O]$ = 2.2 M; 50 °C. Red circles: [**2**] = 1 mM, [PCA] = 5 mM, $[H_2O]$ = 2.2 M; 50 °C. Dashed curve is a theoretical curve calculated in accordance with the kinetic scheme described in Section 3.3. (For interpretation of the references to colour in this figure legend, the reader is referred to the web version of this article.)

vanadium species under the catalytic conditions, into the diperoxo vanadium complexes (Fig. 4A). However, ^{51}V NMR results testify that the major product of this transformation, *viz.* the diperoxo vanadium complex $[VO(OO)(OOH)(pca)]^-$ (**7**), does not participate in the rate-determining step of the oxidation reaction (Figs. 1e, f, and 4B). Indeed, the corresponding resonance H has almost disappeared upon the addition of a 10-fold excess of PCA (see also [79] for **1**), whereas the oxidation rate is decreased only by *ca.* 20–25%. Therefore, the rate-determining step can be ascribed to a transformation of another low-abundant diperoxo vanadium derivative containing one pca-ligand, which is formed from complex **5** upon addition of H_2O_2 in acidic media. We assume that such species is formed by a selective proton delivery to the specific sites in the vanadium coordination sphere resulted in highly unstable radical generators within the catalytic cycle. An increase in the isopropanol oxidation rate at $[PCA]_0$ = 0–0.004 M (Fig. 9) is in agreement with the increase in the **7** concentration, whereas at high initial PCA concentrations (0.006–0.024 M) the reaction rate is decreased due to the increase in the catalyst resting state concentration (**5**).

We propose here a new common kinetic scheme of the isopropanol oxidation in **1**/PCA or **2**/PCA systems which is based on spectroscopic and kinetic data (Scheme 4). Furthermore, using DFT calculations (see below, Section 3.5), we reevaluate our previous findings. Equilibrium transformations in the vanadium precursor/H_2O_2/PCA system in moist isopropanol when $[H_2O_2]_0 \gg [PCA]_0 >$

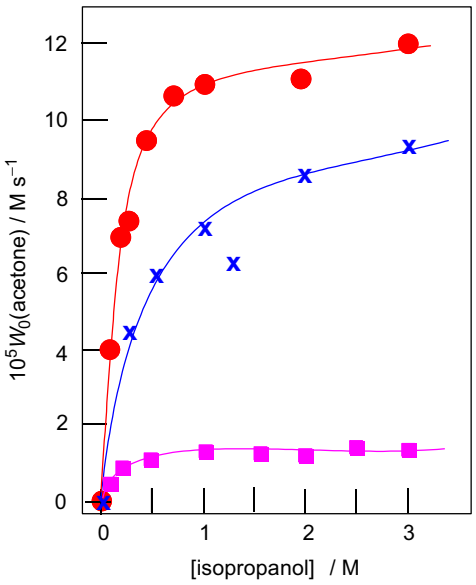

Fig. 11. Dependence of the initial rate of acetone accumulation in isopropanol oxidation in acetonitrile solution on the initial concentration of isopropanol. Blue crosses: [**1**] = 1 mM, $[PCA]_0$ = 4 mM, $[H_2O_2]_0$ = 0.50 M, $[H_2O]$ = 2.2 M, 50 °C. Red circles: [**2**] = 1 mM, [PCA] = 4 mM, $[H_2O_2]_0$ = 0.50 M, $[H_2O]$ = 2.2 M, 50 °C. Pink squares: [**2**] = 0.1 mM, [PCA] = 0.4 mM, $[H_2O_2]_0$ = 0.50 M, $[H_2O]$ = 2.2 M; 50 °C. (For interpretation of the references to colour in this figure legend, the reader is referred to the web version of this article.)

$[\mathbf{2}]_0$ (or $[\mathbf{1}]_0$) (the product formation is low) can be described by the set of Eqs. (1)–(12) (in which pcaH ≡ PCA).

$$[V(O)(OO)_2(H_2O)]^-(\mathbf{8}) + \text{Solvent} \rightleftharpoons [V(O)(OO)_2(\text{Solvent})]^-(\mathbf{9}) + H_2O \qquad K_1 \qquad (1)$$

$$[V(O)(OO)_2(H_2O)]^-(\mathbf{8}) + \text{pcaH} \rightleftharpoons [V(O)(OO)(OOH)(pca)]^-(\mathbf{7}) + H_2O \qquad K_2 \qquad (2)$$

$$[V(O)(OO)_2(\text{Solvent})]^-(\mathbf{9}) + \text{pcaH} \rightleftharpoons [V(O)(OO)(OOH)(pca)]^-(\mathbf{7}) + \text{Solvent} \qquad K_3 \qquad (3)$$

$$[V(O)(OO)(OOH)(pca)]^-(\mathbf{7}) + \text{pcaH} \rightleftharpoons \textit{cis}\text{-}[V(O)(OO)(pca)_2]^-(\mathbf{5}) + H_2O_2 \qquad K_4^{cis} \qquad (4)$$

$$[V(O)(OO)(OOH)(pca)]^-(\mathbf{7}) + \text{pcaH} \rightleftharpoons \textit{trans}\text{-}[V(O)(OO)(pca)_2]^-(\mathbf{6}) + H_2O_2 \qquad K_4^{trans} \qquad (5)$$

$$\textit{cis}\text{-}[V(O)(OO)(pca)_2]^-(\mathbf{5}) + H_3O^+ \rightleftharpoons [V(O)(OO)(H_2O)(pca)](\mathbf{21}) + \text{pcaH} \qquad K_5^{cis} \qquad (6)$$

$$\textit{trans}\text{-}[V(O)(OO)(pca)_2]^-(\mathbf{6}) + H_3O^+ \rightleftharpoons [V(O)(OO)(H_2O)(pca)](\mathbf{21}) + \text{pcaH} \qquad K_5^{trans} \qquad (7)$$

$$[V(O)(OO)(OOH)(pca)]^-(\mathbf{7}) + H_3O^+ \rightleftharpoons [V(O)(OO)(H_2O_2)(pca)](\mathbf{11}) + H_2O \qquad K_6 \qquad (8)$$

$$[V(O)(OO)(H_2O_2)(pca)](\mathbf{11}) + H_2O \rightleftharpoons [V(O)(OO)(H_2O)(pca)](\mathbf{21}) + H_2O_2 \qquad K_7 \qquad (9)$$

$$[V(O)(OO)(H_2O_2)(pca)](\mathbf{11}) \rightleftharpoons [V(OH)(OO)(OOH)(pca)](\mathbf{12}) \qquad K_H \qquad (10)$$

$$\text{pcaH} + H_2O \rightleftharpoons \text{pca}^- + H_3O^+ \qquad K_a \qquad (11)$$

$$[V(OH)(OO)(OOH)(pca)](\mathbf{12}) \rightarrow HOO^{\cdot} \qquad k_{obs} \qquad (12)$$

Eq. (1) was proposed earlier by Conte and co-workers [120,121] to describe the water–isopropanol ligand exchange between two corresponding vanadium diperoxo complexes **8** and **9a**. Starting from **2** as a vanadium source and isopropanol as a solvent K_1 (for the case of **2**; isopropanol) value can be estimated from Fig. 1b using an integration of the corresponding signals G, F and is equal to 0.11. By analogy a value of 0.16 can be obtained for K_1 (case of **1**; isopropanol) from our previous studies (Fig. 5e in [79]) for the vanadate system. The difference between these two values resulted apparently from the different modes of sample preparation (see Section 2). In the case when acetonitrile was used as a solvent the K_1 (**2**; acetonitrile) value can be estimated from Fig. 2b to be 0.10. It means that acetonitrile and isopropanol have close affinities to form the corresponding vanadium diperoxocomplexes **9b** and **9a**. All parameters are summarized in Table 2.

Eqs. (2) and (3) reflect the affinity of added PCA to the vanadium diperoxo complexes **8** and **9** with the subsequent formation of $[V(O)(OO)(OOH)(pca)]^-$ (**7**). In isopropanol solutions of precursor **2** the K_2 and K_3 values can be calculated using the integration of the NMR signals in Fig. 1e and give 330 and 3800, respectively. Thus, the isopropanol ligand is more easily replaced by PCA from the vanadium coordination sphere than the aqua ligand. By analogy, starting from **1** the K_2 and K_3 values can be calculated using the integration of the NMR signals in Fig. 5d from [79] and give 700 and 3100, respectively. Alternatively, K_2 can be determined by using the association constant of **8** and PCA in water [121], considering the experimentally determined pH of the solution (4.68), in this case K_2 = 810. As we can see the estimation of K_2 works well in the case of vanadate precursor, while the water–PCA competition in the vanadium coordination sphere Eq. (2) is poorly estimated in the case of **2**. However, both systems show close parameters for the isopropanol–PCA competition within the vanadium coordination sphere Eq. (3). In aprotic acetonitrile, complex **7** is less stable in contrast to isopropanol solution (where the solvent presumably can stabilize the intermediate by hydrogen bonding), so that we were not able to monitor it by NMR. Therefore, the estimation of K_2 and K_3 values in acetonitrile was not performed.

Eqs. (4) and (5) correspond to a competitive process between PCA and H_2O_2 in the vanadium coordination sphere. In isopropanol, the equilibrium constant K_4^{cis} associated with the major substitution product **5** can be estimated from Fig. 1e using Eq. (13), as being equal to 1200, the concentrations of catalytically active complexes containing one pca-ligand being negligible. By analogy, K_4^{cis} is equal to 880 in the case vanadate was used as a precursor from our previous data (Fig. 5d in [79]).

$$[PCA] = [PCA]_0 - 2[\mathbf{5}] - 2[\mathbf{6}] - [\mathbf{7}] \qquad (13)$$

Compound **6** is the minor substitution product and its concentration under reaction conditions in isopropanol is extremely low. Complex **6** is a labile stereoisomer of **5** where two PCA-ligands are *O-trans* to each other, it was crystallized from aqueous solution of **1** [84]. In isopropanol, the corresponding equilibrium constants K_4^{trans} are small relative to K_4^{cis} and are estimated as 30 from Fig. 1e as well as from Fig. 5d in [79] using the same approach as for the K_4^{cis}. In acetonitrile, the absolute values of K_4^{cis} and K_4^{trans} cannot be determined, however, as soon as $K_4^{cis}/K_4^{trans} = [\mathbf{5}]/[\mathbf{6}]$ the ratio is equal to 7 using the integration of the corresponding signals I and E in Fig. 2e. Thus, the *cis–trans* isomerisation Eqs. (4) and (5) is more important in acetonitrile solution than in isopropanol, where the K_4^{cis}/K_4^{trans} ratio is higher: $[\mathbf{5}] \gg [\mathbf{6}]$.

In our previous studies, the role of water was somehow underestimated as far as in most cases we treated the system as being in

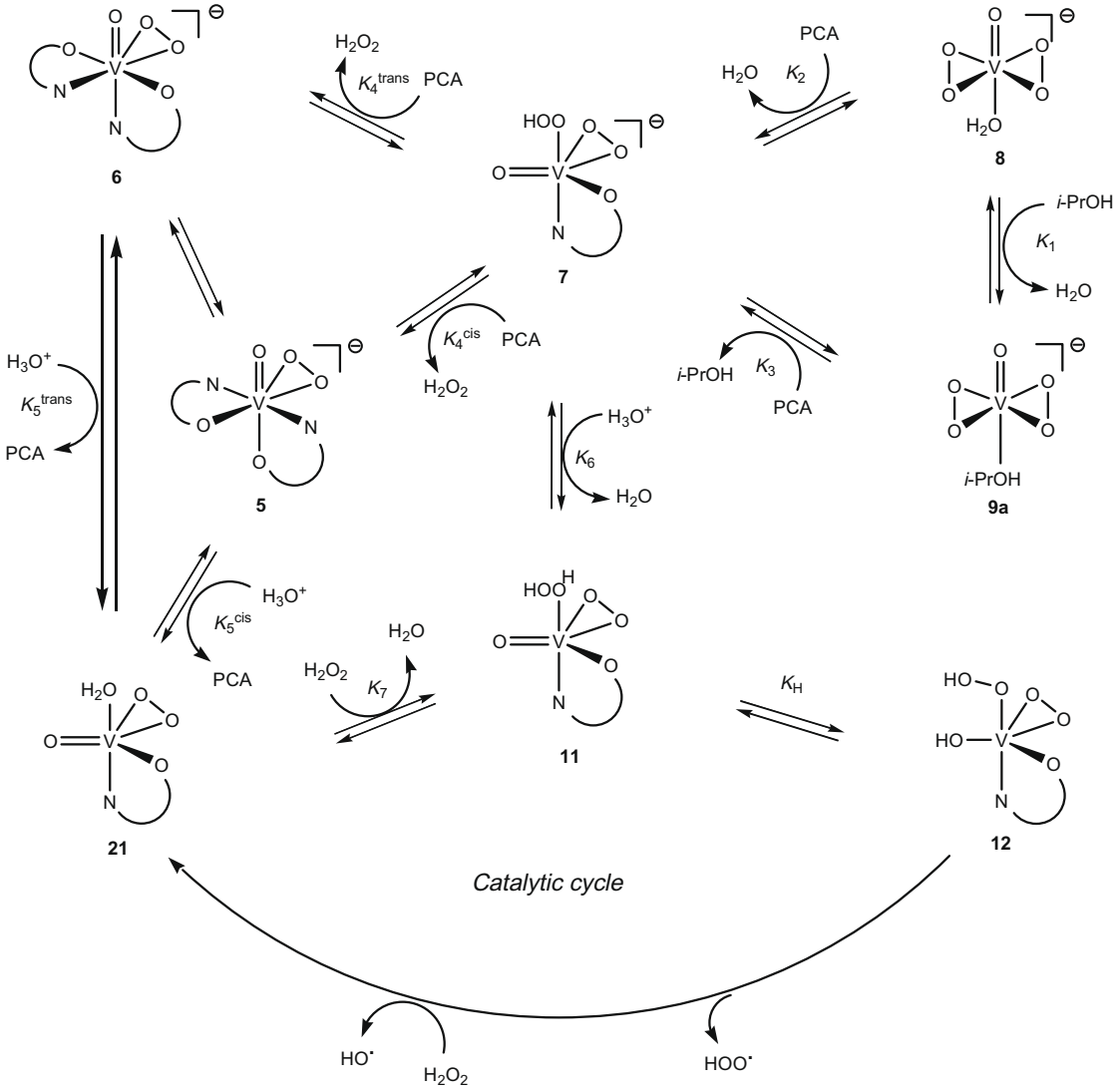

Scheme 4. Equilibria for the **2**–H_2O_2–PCA system in the isopropanol solution.

Table 2
Parameters determined for the mechanism of isopropanol oxidation with H_2O_2 in the presence of the catalytic systems **1**/PCA and **2**/PCA.

Parameter	**1**/PCA in isopropanol[a]	**2**/PCA in isopropanol[a]	**2**/PCA in acetonitrile[b]
K_1 (estimated from spectra)	0.16 (0.17)	0.11 (0.17)	0.10
K_2 (estimated from spectra)	700 (4416)	330 (4416)	nd
K_3 (estimated from spectra)	3100 (3310)	3800 (3310)	nd
K_4^{cis} (estimated from spectra)	880 (5689)	1200 (5689)	nd
K_4^{trans} (estimated from spectra)	30	30	nd
K_5^{cis} (taken from [120–122])	1.25	1.25	1.25
K_5^{trans} (estimated from spectra)	0.03	0.03	0.18
$k_{obs}K_HK_6$ (calculated in accordance with Scheme 4)	8.5×10^4 s^{-1}	1.1×10^5 s^{-1}	nd

[a] Values calculated using DFT method in parentheses (see Section 3.5).
[b] Abbreviation: nd, not determined.

"pure" organic solvents. However, we showed lately [79] that water retards the oxidation of isopropanol presumably due to competing with hydrogen peroxide for the place in the vanadium coordination sphere. From the other hand, the addition of aqueous solution of a strong inorganic acid (e.g. $HClO_4$ [75,91]) resulted in the significant acceleration of the overall oxygenation reaction. It appears water molecules can selectively deliver protons to switch between different intermediates in acidic media. Using our previous results [79] as well as studies by Conte and co-workers on the intermediate **21** [122] we propose that equilibria 6–8 are involved into generation of active species, thus, starting the catalytic cycle (see Scheme 4).

Indeed, the equilibria 6 and 7 describe how protons are delivered by H_3O^+ to the PCA-ligand in **5** and **6** to form **21** by the simple exchange after protonation. These processes have been resumed by Conte [121], and K_5^{trans} was determined to be 1.25. Using the $K_5^{trans}/K_5^{cis} = [\mathbf{5}]/[\mathbf{6}]$ ratio, in isopropanol K_5^{cis} is estimated to be 0.03 for both pre-catalysts **1** and **2**, while in acetonitrile it is equal to 0.18. In equilibrium 8 a proton is formally transferred to the coordinated hydroperoxo group in **7** by H_3O^+ to form a species with a tentative description [V(O)(OO)(H_2O_2)(pca)] (**11**). The exact structure of this intermediate will be discussed in detail below using theoretical calculations, however, we can see that it represents a developed structure of aqua ligand displacement in **21** by a hydrogen peroxide molecule. This process is described by Eq. (9). Species **11** is a key intermediate in the catalytic cycle which allows the proton transfer to the oxo group to form **12** Eq. (10) which is found to generate the HOO· radical in the rate-determining step Eq. (12) [79,101].

Thus, we come up with a new detailed mechanistic scheme for both **1** and **2**. Unlike in the previous studies, we structurally clarify the pre-equilibrium stage Eqs. (1)–(5) based on the spectroscopic observations. Furthermore, we assumed the generation of highly reactive low-abundant species **11**, **12**, **21** *via* selective protonation of these intermediates by H_3O^+ Eqs. (6)–(9) according to the established processes [120–122] and our preliminary tests. The feasibility of the key proton transfer step **11** → **12** being purely speculative at this point was elaborated using theoretical calculations.

According to our scheme, the overall oxidation rate is determined by Eqs. (12) and (14). Taking into account that for the initial reaction rates we can assume $[H_2O_2] \approx [H_2O_2]_0 \gg [PCA]_0$ and $[\mathbf{2}]_0$, only two mass balance equations on PCA Eq. (13) and **2** Eq. (15) can be used in isopropanol solution ($K_4^{cis} \gg K_4^{trans}$; $[\mathbf{5}] \gg [\mathbf{6}]$), which are transformed into Eqs. (16) and (17). The initial oxidation rate is described by Eq. (18), where $[\mathbf{5}]$ can be calculated from the system of Eqs. (16), (17) or determined from the corresponding UV–vis spectra [$\varepsilon_{457}(\mathbf{5}) = 350\ M^{-1}\ cm^{-1}$].

$$W_0 = k_{obs}[\mathbf{12}] \tag{14}$$

$$[\mathbf{2}]_0 = [\mathbf{5}] + [\mathbf{6}] + [\mathbf{7}] + [\mathbf{8}] + [\mathbf{9a}] + [\mathbf{11}] + [\mathbf{12}] + [\mathbf{21}] \approx [\mathbf{5}] + [\mathbf{7}] + [\mathbf{8}] + [\mathbf{9a}] \tag{15}$$

$$[\mathbf{5}] = \frac{[\mathbf{2}]_0}{1 + [H_2O_2]_0/K_4^{cis}[PCA] + [H_2O_2]_0\{[H_2O]_0/K_2 + [i-PrOH]_0/K_3\}/K_4^{cis}[PCA]^2} \tag{16}$$

$$[PCA] = \frac{1}{2}\Big\{[PCA]_0 - 2[\mathbf{5}] + \Big(4[\mathbf{5}]^2 - 4[PCA]_0[\mathbf{5}] + [PCA]_0^2 - 4[\mathbf{5}][H_2O_2]_0/K_4^{cis}\Big)^{1/2}\Big\} \tag{17}$$

$$W_0 = k_{obs}[\mathbf{12}] = k_{obs}\frac{K_H K_6[\mathbf{5}][H_2O_2]_0 K_a^{1/2}}{K_4^{cis}\{[PCA][H_2O]\}^{1/2}} \tag{18}$$

The dissociation constant K_a was obtained using the experimentally determined pH values under the reaction conditions and, for the isopropanol/water 12.4/2.2 M ratio, it shows the value of 7.3×10^{-8}. The $k_{obs}K_HK_6$ value can be determined from Figs. 8–10 fit to be $1.1 \times 10^5\ s^{-1}$.

The same rationale can be used in the case of **1** as a catalyst precursor in isopropanol solution. Treating our previous experimental data [79] (Figs. 13–16) within the scheme proposed we found the $k_{obs}K_HK_6$ value is $8.5 \times 10^4\ s^{-1}$ in this case, which is close to those obtained for **2**/PCA system above. It should be noted that the proposed kinetic scheme of the isopropanol oxidation satisfactorily describes the experimentally observed dependencies (see the curves in Figs. 7–10, calculated from the kinetic data). The calculated distribution of vanadium complexes in moist isopropanol is shown in Fig. 12. The parameters are summarized in Table 2.

3.4. Oxidation of alkanes

Main kinetic features of the cyclohexane oxidation using vanadatrane (**2**) as a catalyst and PCA as a co-catalyst are shown in Figs. S1–S5 (see Supplementary material). It can be seen that the modes of the dependences are the same as they have been previously found for a similar oxidation catalyzed by vanadate (**1**) [75,79]. Thus, the dependence of the initial cyclohexane oxidation rate on the initial concentration of cyclohexane exhibits a plateau at [cyclohexane]$_0$ > 0.2 M (Fig. S3). This mode corresponds to the competition between cyclohexane and acetonitrile for the same oxidative species, *i.e.*, the hydroxyl radical. The dependence of W_0 on the concentration of PCA is depicted with the bell-shaped curve

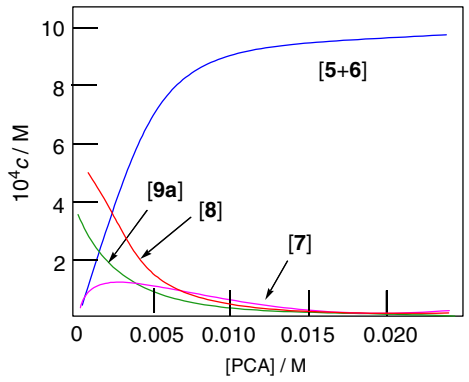

Fig. 12. Distribution of the vanadium-containing species formed from **2** at different concentrations of PCA. Conditions: [**2**] = 1 mM, $[H_2O_2]_0$ = 0.50 M, [*i*-PrOH] = 12.4 M, $[H_2O]$ = 2.2 M.

(Fig. S4). An increase in the rate upon the addition of PCA at its concentration < 5×10^{-4} M testifies that hydroxyl radical generation is associated with the formation of complexes between vanadium-containing species and PCA. Very similar modes of dependences have been found for the oxidation catalyzed by vanadate anion [75].

The selectivity parameters determined for the oxidation of saturated hydrocarbons on vanadatrane **2** (Table 3, entry 1) are close to the parameters determined for the oxidations by the **1**–PCA–H_2O_2 (entry 2) and $NaVO_3$–H_2SO_4–H_2O_2 (entry 3) as well as by systems which oxidize alkanes with the participation of hydroxyl radicals (compare with the parameters summarized in entries 4–8 of Table 4). It is clear that the corresponding selectivity parameters for the systems that do not involve active oxygen-centered radicals (entries 9–11) are noticeably higher. The oxidation of *cis*- and *trans*-1,2-dimethylcyclohexanes proceeds non-stereoselectively as the *trans*/*cis* ratios of isomeric alcohols (after reduction with PPh_3) were *ca.* 1. On the basis of the selectivity parameters, we can assume that the alkane oxidation reactions by both **1**–PCA–H_2O_2 and **2**–PCA–H_2O_2 systems proceed *via* the formation of hydroxyl radicals.

3.5. Theoretical (DFT) study of radical formation

3.5.1. Equilibria in solution

In order to additionally investigate the details of the reaction mechanism and interpret experimental observations, quantum chemical calculations at the DFT level of theory have been performed. First, the equilibrium structures of complexes **5**–**9** detected by NMR in solutions of **1** or **2** in the presence of PCA and/or H_2O_2 have been calculated. For each structure, all possible isomers have been verified and the most stable ones are depicted in Schemes 4 and S1. For complex $[VO(OO)(pca)_2]^-$, another isomer **6** observed in solution was found to be less stable, by 1.9 kcal/mol, than **5** in qualitative agreement with experiment. The calculated equilibrium constants (Table 2) agree well with the experimental values (the difference in the ΔG scale is only 1.1–1.2 kcal/mol) thus confirming the abovementioned interpretation of equilibria in solution.

3.5.2. Catalytic cycles based on monoperoxo-complexes ("cycle I" and "cycle II"). Generation of HOO· radicals

The proposed catalytic cycle for the generation of HOO· and HO· radicals includes the formation of a H_2O_2 V^V complex (**11**) followed by H-transfer to the oxo-ligand and elimination of HOO· to yield the V^{IV} species **15** (Scheme 5). The HO· radical is formed as a result of the reaction of H_2O_2 with this V^{IV} complex and subsequent H-

Table 3
Selectivity parameters in oxidation of alkanes.[a]

Entry	System	C(1):C(2):C(3):C(4)			1°:2°:3°				trans/cis	
		n-Hexane	*n*-Heptane	*n*-Octane	2-Methylhexane	3-Methylhexane	Methylcyclohexane	2,2,4-Trimethylpentane	*cis*-DMCH	*trans*-DMCH
1	**2**– PCA–H_2O_2 (MeCN, 40 °C)	1.0:4.0:4.4	1.0:5.5:6.0:5.1	1:0:4.1:3.9:3.8	1.0:3.8:9.9	1.0:4.1:8.0	1:4:10	1.0:4.3:4.9	0.70	0.75
2	**1**–PCA–H_2O_2 (MeCN, 40 °C)	1:8:7	1:9:7:7	1:7:7.5:5	1:14:64	1:6:22	1:6:18	1:4:9	0.75	0.80
3	**1**–H_2SO_4–H_2O_2 (MeCN, 50 °C)[b]		1:7:6.5:6.5	1:10:10.5:8.5			1:7:26		0.85	0.90
4	*hν*–H_2O_2 (MeCN, 20 °C)	1:10:7	1:7:6:7			1:4:12		1:2:6	0.9	
5	$FeSO_4$–H_2O_2 (MeCN, 20 °C)		1:5:5:4.5					1:3:6	1.3	
6	$Fe(ClO_4)_3$–H_2O_2 (MeCN, 20 °C)	1:9: 9				1:4:30	1:7:43	1:5:13		
7	$Ni(ClO_4)_4$–H_2O_2 (MeCN, 70 °C)[c]		1:6.3:7.2:6.1			1:5.3:55	1:7:15	1:2.3:4.5		
8	**I**-H_2O_2 (MeCN, 60 °C)[d]	1:6.2:7.1	1:5.5:5.0:4.6		1:6:19		1:4:10	1:5:8.5	0.9	
9	$NaAuCl_4$–H_2O_2 (MeCN, 75 °C)[e]		1 : 35:25:23		1:13:100		1:116:255	1:10:240		
10	**II**–$MeCO_2H$–H_2O_2 (MeCN, 25 °C) [f]	1:46:35:34	1:29:25:24	1:19:204	1:22:200	1:26:200	1:5:55	0.34	4.1	
11	*m*-CPBA (MeCN, 25 °C)[g]	1:36:36.5					1:89:750	1:20:520	0.65	

[a] All parameters were measured after reduction of the reaction mixtures with triphenylphosphine before GC analysis and calculated based on the ratios of isomeric alcohols. The parameters calculated from the concentrations of alcohols after reduction with PPh_3 were normalized, *i.e.*, calculated taking into account the number of hydrogen atoms at each carbon. Parameters C(1):C(2):C(3):C(4) are relative reactivities of hydrogen atoms at carbons 1, 2, 3, and 4 of the *n*-heptane or *n*-octane chain. Parameters 1°:2°:3° are relative normalized reactivities of the hydrogen atoms at primary, secondary, and tertiary carbons of branched alkanes. Parameter *trans*/*cis* is determined as the ratio of the formed tertiary alcohol isomers with mutual *trans* and *cis* orientation of the methyl groups. Abbreviations: MCH is methylcyclohexane; *cis*-DMCH and *trans*-DMCH are isomers of 1,2-dimethylcyclohexane.
[b] For this system, see [92].
[c] In the presence of TMTACN (1,4,7-trimethyl-1,4,7-triazacyclononane). For this system, see [124].
[d] Compound **I** is the complex (2,3-*η*-1,4-diphenylbut-2-en-1,4-dione)undecacarbonyl triangulotriosmium. For this system, see Ref. [125].
[e] For this system, see Ref. [126].
[f] Compound **II** is the complex $[Mn_2L_2(\mu\text{-}O)_3]^{2+}$ where L is 1,4,7-trimethyl-1,4,7-triazacyclononane. For this system, see Refs. [127–130].
[g] *m*-Chloroperoxybenzoic acid.

Table 4
Energetic characteristics (in kcal/mol) of the reactions discussed in the text.[a]

	$\Delta H_s^{\neq}$	$\Delta G_s^{\neq}$	ΔH_s	ΔG_s
8 + *i*-PrOH → **9a** + H_2O			+0.3[b]	+1.0[b]
8 + PCA → **7** + H_2O			−6.3[b]	−5.0[b]
9a + PCA → **7** + *i*-PrOH			−6.6[b]	−6.0[b]
7 + PCA → **5** + H_2O_2			−6.3[b]	−5.1[b]
11 → **12**, **$TS_{11\text{-}12}$**	21.3	21.5	+5.4	+5.5
TS_{11-12,H_2O}	2.3	10.5	+5.4	+5.5
11 → **13**, **$TS_{11\text{-}13}$**	19.0	19.4	+7.8	+6.2
TS_{11-13,H_2O}	3.9	12.2	+7.8	+6.2
11 → **14**, **$TS_{11\text{-}14}$**	19.7	20.1	+11.8	+10.7
TS_{11-14,H_2O}	3.7	11.3	+11.8	+10.7
12 → **15** + HOO·			+22.3	+12.3
13 → **16** + HOO·			+20.9	+13.0
11 → **15** + HOO·			+27.7	+17.9
11 → **16** + HOO·			+28.8	+19.3
15 + H_2O_2 → **17**			−6.6	+2.0
16 + H_2O_2 → **18**			−8.9	−1.1
17 → **19b** **$TS_{17\text{-}19b}$**	12.7	13.9	+1.5	+1.4
TS_{17-19b,H_2O}	−1.4	6.9	+1.5	+1.4
19b → **19a**			−10.2	−9.7
17 → **20** **$TS_{17\text{-}20}$**	14.0	15.0	−2.5	−3.8
TS_{17-20,H_2O}	3.1	11.5	−2.5	−3.8
18 → **20** **$TS_{18\text{-}20}$**	28.9	29.3	−1.1	−2.0
TS_{18-20,H_2O}	3.4	12.5	−1.1	−2.0
19a → **21** + HO· **$TS_{19a\text{-}21}$**	5.2	5.8	−1.6	−7.9
20 → **22** + HO· **$TS_{20\text{-}22}$**	8.1	8.2	−2.9	−8.4
22 → **21**			−4.9	−4.0
21 + H_2O_2 → **11** + H_2O			+3.9	+4.7
12 → **23** **TS_{12-23,H_2O}**	4.2	12.4	+0.5	+0.5
23 + H_2O_2 → **24** + H_2O			+6.5	+6.0
24 → **25** **TS_{24-25,H_2O}**	0.4	10.3	−9.8	−8.5
25 → **26** + HOO·			+19.9	+10.4
26 + H_2O_2 → **27**			−6.2	+2.0
27 → **28** **TS_{27-28,H_2O}**	4.0	12.0	+3.1	+2.2
28 → **13** + HO· **$TS_{28\text{-}13}$**	8.3	7.6	+3.2	−3.6
11′ + H_2O_2 + PCA → **TS_{17-19b,H_2O}** + HOO· + $NCCH_3$				+15.9
11′ + H_2O_2 + H_2O → **$TS_{17'-19b',H_2O}$** + HOO·				+25.5

[a] Energies given for CH_3CN as solvent unless stated otherwise.
[b] Energies given for isopropanol as solvent.

transfer. This catalytic cycle was *in part* theoretically studied by Bell and co-workers [101]. However, some important details of this mechanism remain unclear.

A first question concerns the stage of H-transfer from the coordinated hydrogen peroxide to the oxo-ligand in complex **11**. Previously [75] it was proposed by some of us that this H-transfer occurs first to the pca-ligand with the cleavage of a metal–ligand bond and only then to the oxo-ligand ("robot's arm" mechanism). Theoretical calculations [101] confirmed that such stepwise pathway *via* the 4-membered transition state (**a**) (Scheme 6) is by 4.3 kcal/mol more favorable than the one-step H-transfer *via* TS (**b**). Moreover, recent results indicated that the oxidation of alkanes can be catalyzed by some metal oxides [51] and $NaVO_3$–H_2SO_4 (or oxalic acid)–H_2O_2 systems [92] without the addition of PCA or any other *N*,*O*-ligands which could facilitate the H-transfer. For example, although the addition of PCA improves the hydrocarbon oxidation catalyzed by the methyltrioxorhenium–H_2O_2 system [97–99], recent experiments [51] and DFT calculations [102] showed that this system is also active without any *N*,*O*-species.

Here we propose one more efficient pathway for this proton migration in the vanadium complex. Since the oxidation occurs in the presence of water which molecules are strongly polar, H_2O may be directly involved in the H-transfer process, being part of a corresponding transition state. Such TS (**c**) (Scheme 6) bears a six-membered metallacycle and, hence, is expected to be more stable than both four-membered TSs (**a**) and (**b**). Indeed, our calcula-

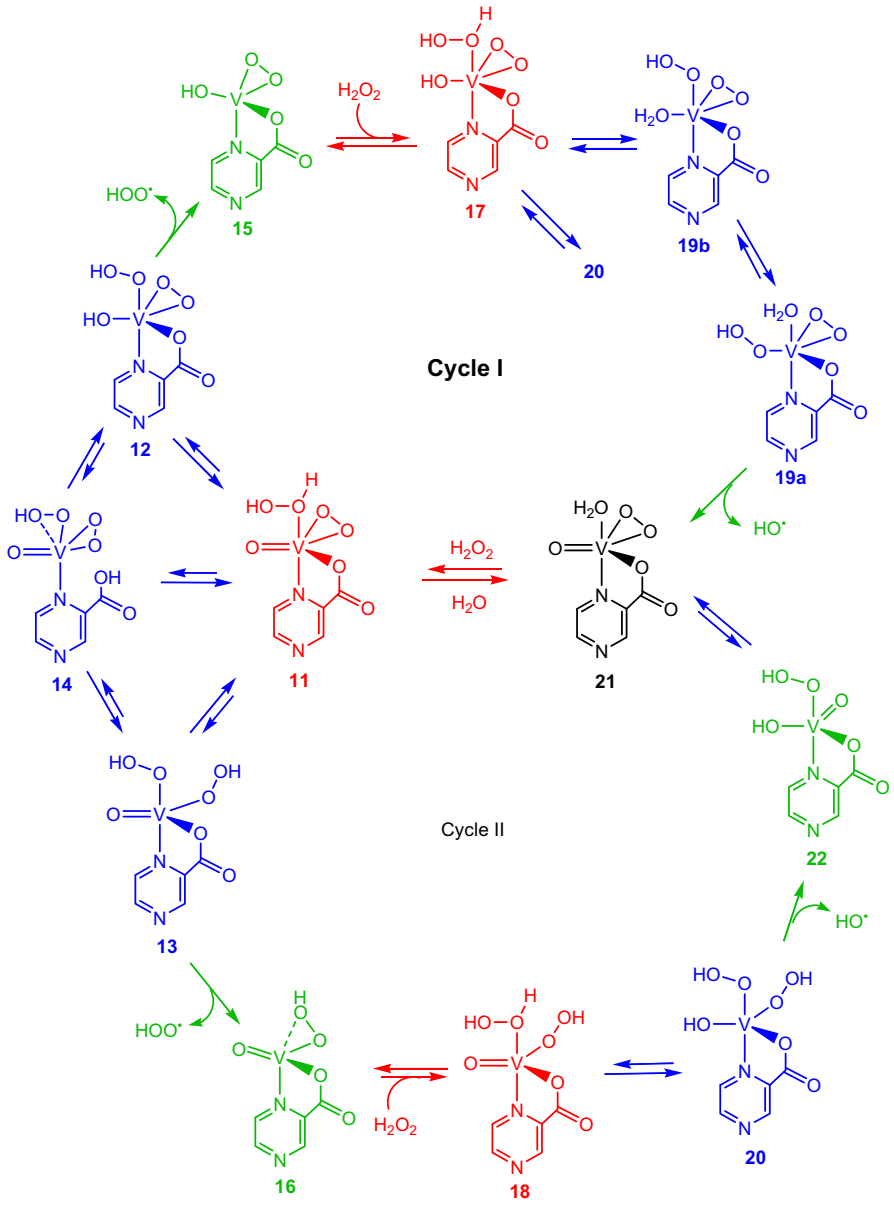

Scheme 5. Catalytic cycles for the formation of HOO· and HO· radicals based on monoperoxo-complexes: "Cycle I" (the most favorable one) and "Cycle II". Color code: red – formation of H_2O_2-adducts, blue – H-transfers, green – radical generation. (For interpretation of the references to colour in this scheme legend, the reader is referred to the web version of this article.)

tions indicate the following. First, water-assisted H-transfers to oxo-, peroxo-, or pca-ligands (**11** → **12**, **11** → **13**, or **11** → **14**, Scheme 5) *via* $\mathbf{TS_{11-12,H_2O}}$, $\mathbf{TS_{11-13,H_2O}}$ or $\mathbf{TS_{11-14,H_2O}}$ [type (**c**), Fig. 13] have significantly (by 7.2–11.1 kcal/mol, Table 4) lower activation barriers than the corresponding H-transfers via four-membered $\mathbf{TS_{11\text{-}12}}$, $\mathbf{TS_{11\text{-}13}}$, or $\mathbf{TS_{11\text{-}14}}$ [types (**a**) and (**b**)]. Such a role of water as a H-transfer promoter is in agreement with results of the recent theoretical studies of the mechanism of alkane oxidations catalyzed by methyltrioxorhenium complex [$MeReO_3$] in the presence of aqueous H_2O_2 [102] and of halide ion oxidations catalyzed by a vanadium haloperoxidase [131]. Second, proton migration to the oxo-ligand initiates "cycle I" and has the lowest activation barrier while that to the peroxo-ligand that starts "cycle II" requires the highest energy. However, the difference of the $\Delta G_s^{\neq}$ values for these three channels is small and does not exceed 1.7 kcal/mol. Therefore, all three proton transfers have a similar probability from the kinetic viewpoint. Third, gas-phase E_a and $\Delta H^{\neq}$ values of the water-assisted pathways are negative. Such a situation was described previously for some cycloaddition reactions [132–134], and it is caused by the formation, on the first step of the process, of a molecular van der Waals complex between **11** and H_2O with a total energy lower than the sum of the total energies of separated **11** and water. The consideration of the entropic factor and solvent effects increases activation barriers and the $\Delta G_s^{\neq}$ values become positive. In fact, the activation barriers of these reactions are determined by entropic contribution and solvation rather than by enthalpic contribution. Fourth, the products with protonated oxo- and peroxo-ligands (**12** and **13**) have a similar thermodynamic stability while the complex **14** with protonated pca-ligand is by 4.5–5.1 kcal/mol less stable.

It is important to note that the now proposed water-assisted mechanism does not contradict with the experimental results that indicate a decrease in the reaction rate with an increase in the water concentration. Indeed, the experimental "reaction rate-water concentration" relationship is accounted for by equilibrium **11** ⇆ **21**: enhancement of the H_2O concentration shifts this equi-

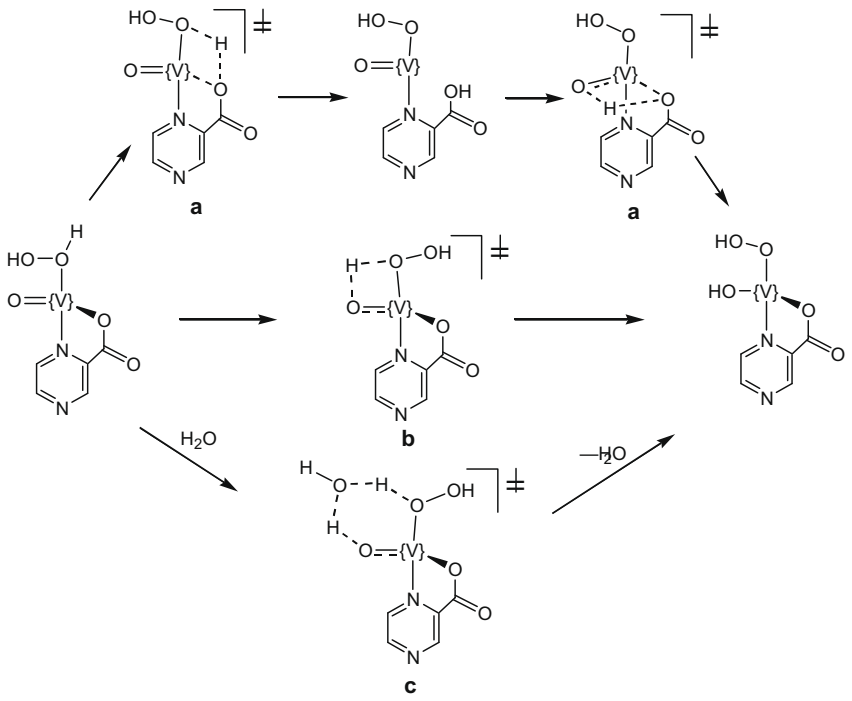

Scheme 6. Mechanisms of H-transfers *via* 4-membered (**a**, **b**) and 6-membered (**c**) transition states. Coordinated peroxo group is omitted for clarity.

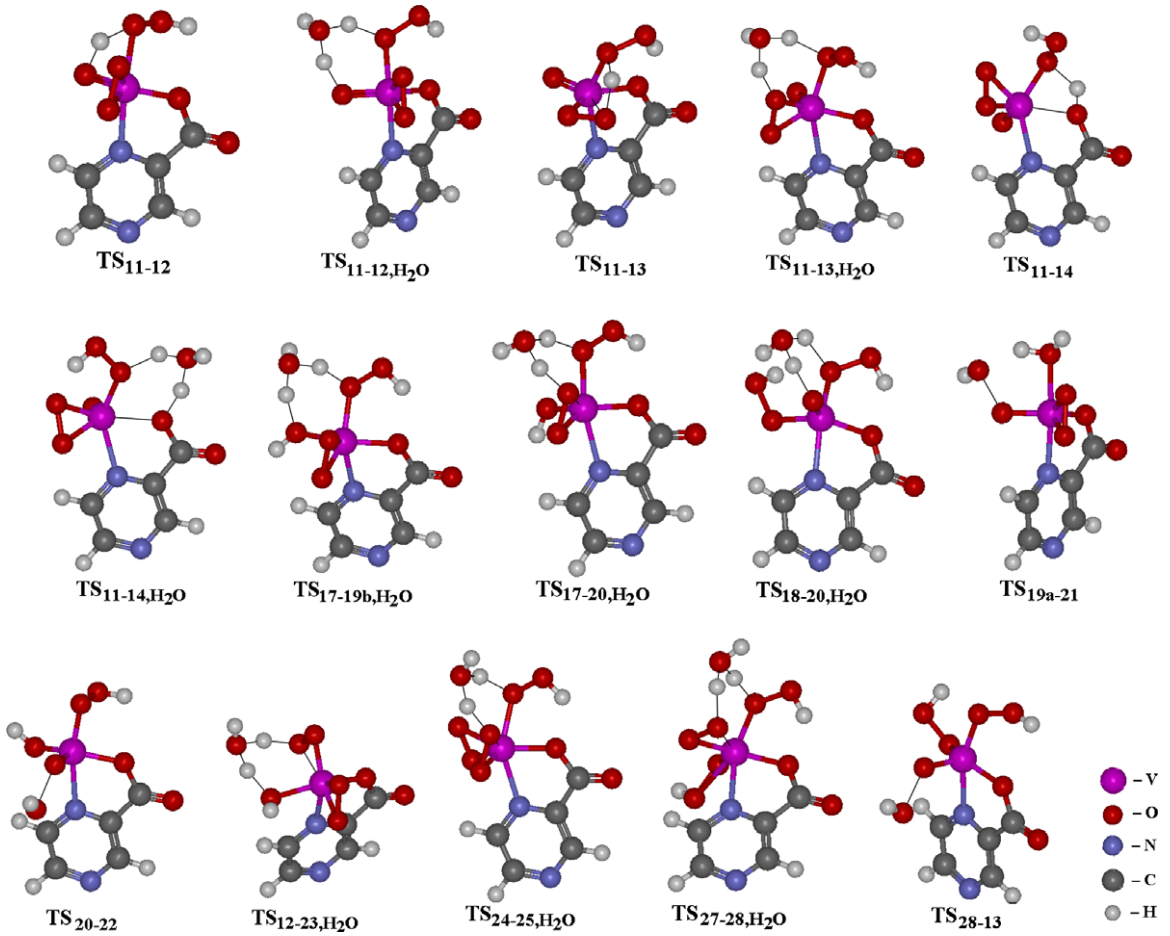

Fig. 13. Equilibrium structures of some calculated transition states.

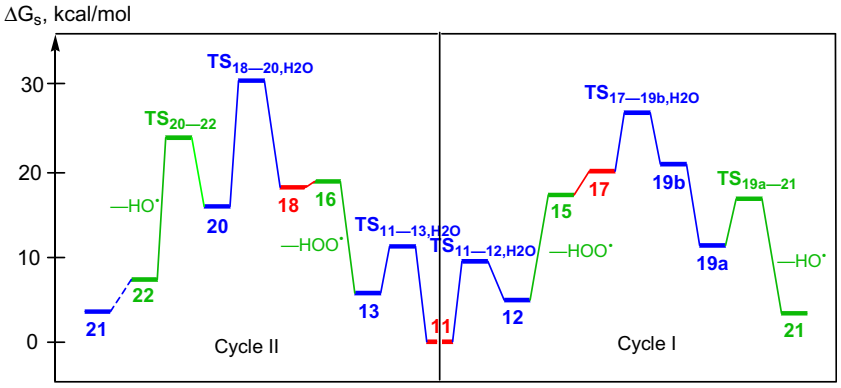

Fig. 14. Energy profiles of the catalytic "cycle I" and "cycle II". For color code, see Scheme 6.

librium toward **21** and decreases the concentration of **11**, the active species of the catalyst.

The next step of the catalytic cycles consists of the unimolecular elimination of the HOO· radical from complex **12** or **13** to give the V^{IV} species **15** or **16**, respectively. It is worthwhile to mention that no transition state for S_N2 replacement of HOO· with H_2O_2 was found either by us or by Bell and co-workers [101]. The calculated ΔG_s values of reactions **12** → **15** and **13** → **16** (that is, the adiabatic V–OOH bond energies) are similar (12.3 and 13.0 kcal/mol, respectively, Table 4). An apparent ΔG_s value of the formation of **15** + HOO· relative to **11** (*i.e.*, the active species initiating the whole catalytic cycle) is by 1.4 kcal/mol lower than that of the formation of **16** + HOO· (Fig. 14). Thus, the generation of HOO· radical in the "cycle I" is slightly more plausible than that in "cycle II".

3.5.3. Catalytic cycles based on monoperoxo-complexes ("cycle I" and "cycle II"). Generation of HO· radicals

One more important question which was not yet studied theoretically concerns the energetic features and details of the final stage, that is the HO· radical generation. This stage starts with the formation of the hydrogen peroxide adducts **17** or **18** upon the addition of H_2O_2 to **15** or **16**. For both complexes **17** and **18** several possible isomers have been found and only the most stable ones are discussed further. The reactions are exothermic (by −6.6 and −8.9 kcal/mol, respectively, Table 4) but endoergonic (by 2.0 kcal/mol) or only slightly exoergonic (by −1.1 kcal/mol) due to the decrease in entropy. Complex **17** may further undergo H-transfers from coordinated H_2O_2 either to the hydroxo-ligand (**17** → **19b**) or to the peroxo-ligand (**17** → **20**) whereas in the case of complex **18** proton migration to the oxo-ligand (**18** → **20**) may occur. For all these H-transfers, the water-assisted mechanisms are also more favorable than the direct proton-migrations. Among these three reaction channels, route **17** → **19b** is kinetically the most favorable and results in the formation of the second stable isomer **19b** which then is transformed to the most stable isomer **19a**. Complex **19a** is by 4.5 kcal/mol more stable than **20** and, therefore, route **17** → **19b** → **19a** is also more thermodynamically favorable than the routes leading to **20** (Fig. 14) (an H-transfer to the pca-ligand in complex **17** has an activation barrier 3.4 kcal/mol higher than the H-transfer to the OH-ligand).

The next step of the mechanism is the generation of HO· radicals upon O–O(H) bond cleavage in **19a** or **20**. For this process, transition states $\mathbf{TS_{19a\text{-}21}}$ and $\mathbf{TS_{20\text{-}22}}$ have been located, and the formation of HO· from **19a** is more kinetically preferable, by 2.4 kcal/mol, than that from **20**. Furthermore, the product **21** is thermodynamically more stable than structure **22** by 4.0 kcal/mol. Thus, "cycle I" (Scheme 5) provides a more favorable pathway for the formation of HO· radicals than "cycle II".

3.5.4. Catalytic cycle based on diperoxo-complexes ("cycle III")

Another catalytic cycle leading to the generation of free radicals is based on the diperoxo-complex **24** derived from **12** (formed from **11** upon H-transfer from a H_2O_2 ligand) via **23** as a result of H-transfer from the OOH-ligand to the OH-ligand and following replacement of H_2O with H_2O_2 (Scheme 7). The following proton migration in **24** results in the formation of **25**. The $\Delta G_s^{\neq}$ values of these "water-assisted" H-transfers via $\mathbf{TS_{12-23,H_2O}}$ and $\mathbf{TS_{24-25,H_2O}}$ are 12.4 and 10.3 kcal/mol, close to activation barriers of similar processes discussed above (Table 5).[1] It is interesting that the rate-limiting stage of HOO· generation in "cycle III" is the proton migration **24** → **25** rather than the monomolecular decomposition of **25** (Fig. 15). The formation of HOO· along "cycle III" is less favorable than along "cycle I" because the energy of $\mathbf{TS_{24-25,H_2O}}$ relative to **11** is by 4.5 kcal/mol higher than the energy of the level **15** + HOO· relative to **11**. The generation of HO· radicals may occur via the sequence **26** + H_2O_2 → **27** → **28** → **13** + HO· which also includes the transition states $\mathbf{TS_{27-28,H_2O}}$ (water-assisted H-transfer) and $\mathbf{TS_{28\text{-}13}}$ (monomolecular decomposition of **28**).

3.5.5. Activation energy

In accordance with the previous proposals [75], the reaction mechanism may be represented in a simplified form by the sequence of reactions (19)–(21):

$$\{V^V\}(PCA) + H_2O_2 \leftrightarrows \{V^V\}(PCA)H_2O_2 \quad (19)$$

$$\{V^V\}(PCA)H_2O_2 \rightarrow \{V^{IV}\}(PCA) + HOO^{\cdot} \quad (20)$$

$$\{V^{IV}\}(PCA) + H_2O_2 \rightarrow \{V^V\}(PCA) + HO^{\cdot} \quad (21)$$

where the first species $\{V^V\}(PCA)$ is an active form of the catalyst. The results described in this work and also those obtained by Bell and co-workers [101] suggest that the active form of the catalyst $\{V^V\}(PCA)$ which initiates the catalytic cycle is complex $[V(O)(OO)(pca)(H_2O_2)]$ (**11**) rather than the dioxo-species $[V(O)_2(pca)]$.

It was also proposed [75] that the rate-limiting stage of the HO· radical formation (and hence of the overall process of alkane oxidation) is a monomolecular decomposition of a vanadium hydrogen peroxide adduct [reaction (20)]. However, the analysis of the calculated energy profiles (Figs. 14 and 15) indicates that the rate-limiting stage is H-transfer in V^{IV} complexes **17** ("cycle I") or **27** ("cycle III") (steps **17** → **19b** and **27** → **28**). The stages of unimolecular HOO· eliminations (**12** → **15** + HOO and **25** → **26** + HOO·) or

[1] Herein and in the further discussions we do not consider unimolecular H-transfers *via* four-membered transition states because, as it was indicated above, this would require significantly higher activation barriers.

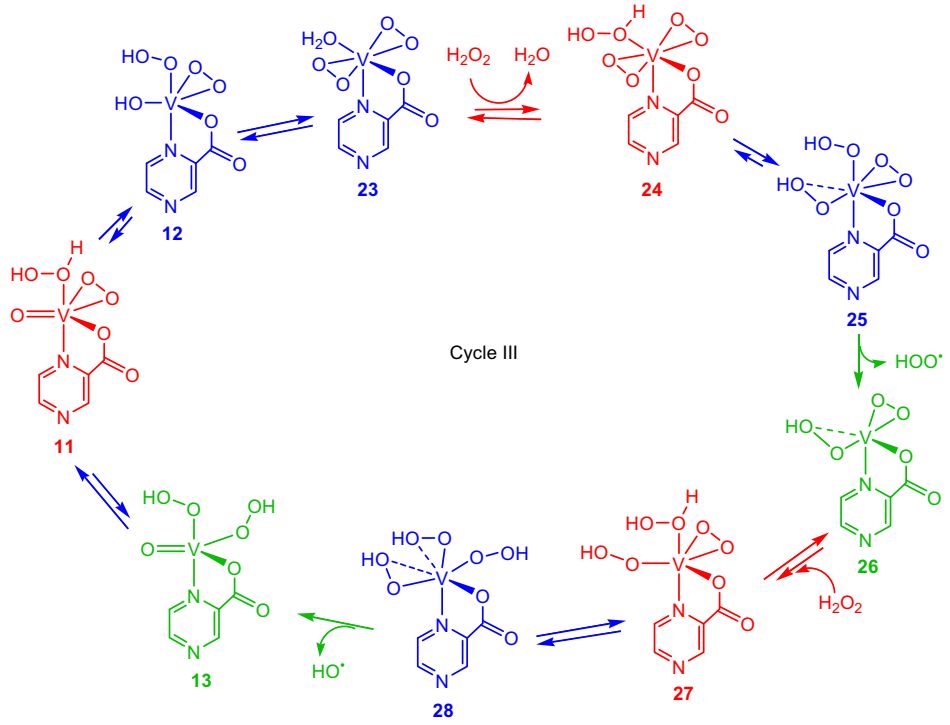

Scheme 7. Catalytic cycle for the formation of HOO· and HO· radicals based on diperoxo-complexes ("Cycle III"). For color code, see Scheme 5.

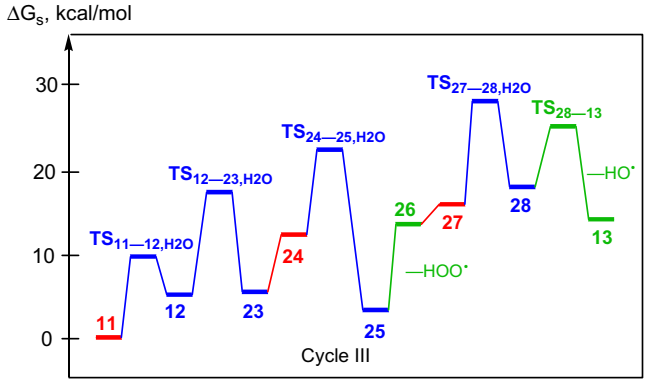

Fig. 15. Energy profile of the catalytic "cycle III". For color code, see Scheme 6.

HO· eliminations (**19a** → **21** + HO· and **28** → **13** + HO·) are less energetically demanding.

The generation of HO· radicals in the "cycle I" is *more* favorable (by 1.3 kcal/mol) than that in the "cycle III". The calculated apparent activation enthalpy of the overall reaction $\Delta H^{\neq}_{s,ap}$ (*i.e.*, difference between enthalpies of the transition state $\mathbf{TS_{17-19b,H_2O}}$ and the active form of the catalyst starting the catalytic cycle **11**) is 19.8 kcal/mol, which is in reasonable agreement with the experimentally determined activation energy of 17 ± 2 kcal/mol [75].

In this work, the involvement of only one water molecule in the H-transfer processes is considered. In real aqueous systems, the proton shifts may be assisted by water clusters bearing several H_2O molecules. In this case, the formation of additional stabilizing H-bonds between the H_2O-cluster and a substrate should further reduce the activation barrier of these steps and, hence, the overall apparent activation energy of the whole reaction providing an even better agreement with the experimental data. At the same time, the H-transfer **17** → **19b** remains to be rate limiting due to the higher energy of **17** compared to **15** (see Fig. 14, Cycle I).

3.5.6. On the possible role of PCA

Finally, another question concerning the reaction mechanism is the role of PCA. Previously [75] it was assumed that without pca-ligand the H-transfer from H_2O_2 to the oxo-ligand should be the rate limiting stage with a high activation energy while an addition of pca-ligand should facilitate the proton migration and decrease the overall activation barrier. However, in the frames of the water-assisted mechanism of H-transfers, the pca-ligand cannot be considered as a promoter of this stage. Here we propose that the role of the pca-ligand is to stabilize of V^{IV} species involved in the rate-limiting step, first of all $\mathbf{TS_{17-19b,H_2O}}$ – the species with the highest energy on the reaction pathway. In order to verify this hypothesis, complexes [V(O)(OO)(H_2O_2)(OH)($NCCH_3$)] (**11′**), [V(OO)(OH)(H_2O_2)(OH)($NCCH_3$)] (**17′**), [V(OO)(OOH)(H_2O)(OH)-($NCCH_3$)] (**19a′**) bearing OH and $NCCH_3$ ligands (shown as the last ones in these formulae) instead of pca, and the corresponding transition state $\mathbf{TS_{17'-19b',H_2O}}$ (*i.e.*, the species which should be involved into the catalytic cycle in the absence of PCA) have been calculated. The results indicate that an addition of PCA to the reaction mixture indeed decreases the apparent activation barrier. The Gibbs free energy of $\mathbf{TS_{17'-19b',H)2O}}$ relative to **11′** is by 9.6 kcal/mol higher than ΔG_s of $\mathbf{TS_{17-19b,H_2O}}$ relative to **11′** (Table 4).

4. Conclusions

We propose here a new common kinetic scheme for oxidations with H_2O_2 in the **1**/PCA and **2**/PCA systems. Detailed spectroscopic and kinetic studies suggest we deal with the same-type intermediates for both pre-catalysts: mono and diperoxovanadium complexes with identified structures. In the case of **2,** the first stage of the reaction is elimination of the triethanolaminate ligand under the action of PCA and H_2O_2. The preequilibrium stages reveal a competitive behavior among H_2O_2, PCA, and water molecules in the vanadium coordination sphere. The proposed scheme satisfactorily describes the experimental data: these catalytic systems activate C–H bonds *via* the same radical generation pathway.

Using DFT calculations, intimate details of the mechanism of free radical generation in the catalytic system under consideration were explored and important modifications to the previous mechanistic proposals are recognized. The main theoretical results include the following: (1) a water-assisted mechanism of proton transfer steps (involving six-membered metallacyclic TSs) is suggested and proved to be even more effective than the "robot's arm" mechanism; (2) the HO· radicals generation in the catalytic cycle is considered in detail for the first time and includes the addition of H_2O_2 to a V^{IV} complex followed by an H-transfer to the hydroxo-ligand, isomerization, cleavage of the O–OH bond to give HO·, and replacement of H_2O by H_2O_2 to regenerate the catalyst; (3) the rate limiting stage of the overall process is the above H-transfer from ligated H_2O_2 to the hydroxo-ligand and not the unimolecular elimination of HOO· radicals; (4) a new role of pca-ligand as a stabilizer of transition state V^{IV} species involved into the rate-limiting stage is proposed; (5) the formation of both HOO· and HO· radicals is more favorable along the cycle based on monoperoxo-complexes ("cycle I") than in the cycle based on diperoxo species ("cycle III"); and (6) the equilibrium structures of V-complexes detected spectroscopically in solution were calculated, as well as the equilibrium constants involving their reactions which are shown to agree with the experimental values, thus confirming the proposed interpretation of equilibria in solution.

It is also noteworthy to refer that this study points out to a considerable generality of the relevant role of water as a promoter of H-transfer in fundamental steps towards the generation of HO· and HOO· radicals, thus extending to the vanadate and vanadatrane systems the behavior recently found [102] for another alkane oxidation system based on quite a different catalyst, the methyltrioxorhenium complex [$MeReO_3$]. Such an important behavior of water deserves to be further explored and searched for other oxidation systems based on the use of H_2O_2 as oxidant.

Acknowledgments

The authors thank the Fundação para a Ciência e a Tecnologia (FCT) and its POCI 2010 programme (FEDER funded) (Grant BPD/34926/07 for M.V.K.) and the Russian Foundation for Basic Research (Grant 06-03-32344-a) for support. M.L.K. is grateful to the FCT and IST for a research contract within the Ciência 2007 scientific programme. The authors thank Dr. A.A. Nazarov and the computer center of the University of Vienna for technical support and computer time at the Linux-PC cluster Schroedinger III. L.S.S. and G.B.S. express their gratitude to the FCT for making it possible for them to stay at the Instituto Superior Técnico, TU Lisbon, as invited scientists and to perform a part of the present work.

Appendix A. Supplementary data

The online version of this article contains additional supplementary material (Scheme S1, Figs. S1–S5, Table S1 with total energies, enthalpies, Gibbs free energies and entropies). Supplementary data associated with this article can be found, in the online version, at doi:10.1016/j.jcat.2009.08.006.

References

[1] J.J.R. Fraústo da Silva, R.J.P. Williams, The Biological Chemistry of the Element, Oxford University Press, Oxford, 2001.
[2] D.C. Crans, J.J. Smee, E. Gaidamauskas, L. Yang, Chem. Rev. 104 (2004) 849–902.
[3] S. Raugei, P. Carloni, J. Phys. Chem. B 110 (2006) 3747–3758.
[4] P.C. Wilkins, M.D. Johnson, A.A. Holder, D.C. Crans, Inorg. Chem. 45 (2006) 1471–1479.
[5] J. Borden, D.C. Crans, J. Florián, J. Phys. Chem. B 110 (2006) 14988–14999.
[6] Y. Zhang, X.-D. Yang, K. Wang, D.C. Crans, J. Inorg. Biochem. 100 (2006) 80–87.
[7] H. Fickl, A.J. Theron, H. Grimmer, J. Oommen, G.J. Ramafi, H.C. Steel, S.S. Visser, R. Anderson, Free Radic. Biol. Med. 40 (2006) 146–155.
[8] A.S. Tracey, G.R. Willsky, E.S. Takeuchi, Vanadium Chemistry, Biochemistry, Pharmacology and Practical Applications, CRC Press, Boca Raton, 2007.
[9] D. Rehder, Bioinorganic Vanadium Chemistry, Wiley, Chichester, 2008.
[10] E.J. Baran, Chem. Biodivers. 5 (2008) 1475–1484.
[11] J.A. Meyer, D.M. Spence, Metallomics 1 (2009) 32–41.
[12] A. Butler, M.J. Clague, G.E. Meister, Chem. Rev. 94 (1994) 625–638.
[13] V. Conte, F. Di Furia, G. Licini, Appl. Catal. A 157 (1997) 335–361.
[14] G. Rothenberg, J.H. Clark, Org. Process Res. Dev. 4 (2000) 270–274.
[15] C. Bolm, Coord. Chem. Rev. 237 (2003) 245–256.
[16] J.-M. Brégeault, J. Chem. Soc., Dalton Trans. (2003) 3289–3302.
[17] J.-M. Brégeault, M. Vennat, L. Salles, J.-Y. Piquemal, Y. Mahha, E. Briot, P.C. Bakala, A. Atlamsani, R. Thouvenot, J. Mol. Catal. A 250 (2006) 177–189.
[18] E. Hoppe, C. Limberg, B. Ziemer, Inorg. Chem. 45 (2006) 8308–8317.
[19] K. Kustin, J.C. Pessoa, D.C. Crans (Eds.), Vanadium: The Versatile Metal, ACS Symposium Series, vol. 974, ACS, Washington, DC, 2007.
[20] P.J. Figiel, J.M. Sobczak, New J. Chem. 31 (2007) 1668–1673.
[21] W. Trakarnpruk, P. Hoonsart, Chin. J. Catal. 28 (2007) 290–292.
[22] H. Hirao, D. Kumar, H. Chen, R. Neumann, S. Shaik, J. Phys. Chem. C 111 (2007) 7711–7719.
[23] P.P. Knops-Gerrits, C.A. Trujillo, B.Z. Zhan, X.Y. Li, P. Rouxhet, P.A. Jacobs, Top. Catal. 3 (1996) 437–449.
[24] A.E. Shilov, G.B. Shul'pin, Chem. Rev. 97 (1997) 2879–2932.
[25] A. Kozlov, K. Asakura, Y. Iwasawa, J. Chem. Soc., Faraday Trans. 94 (1998) 809–816.
[26] A. Kozlov, A. Kozlova, K. Asakura, Y. Iwasawa, J. Mol. Catal. A 137 (1999) 223–237.
[27] A.E. Shilov, G.B. Shul'pin, Activation and Catalytic Reactions of Saturated Hydrocarbons in the Presence of Metal Complexes, Kluwer Academic Publishers, Dordrecht, 2000.
[28] P.M. Reis, J.A.L. Silva, J.J.R. Fraústo da Silva, A.J.L. Pombeiro, Chem. Commun. (2000) 1845–1846.
[29] G. Süss-Fink, L. Gonzalez, G.B. Shul'pin, Appl. Catal. A 217 (2001) 111–117.
[30] G.B. Shul'pin, J. Mol. Catal. A 189 (2002) 39–66.
[31] G.B. Shul'pin, Comptes Rendus Chimie 6 (2003) 163–178 (in English).
[32] G.B. Shul'pin, Oxidations of C–H compounds catalyzed by metal complexes, in: M. Beller, C. Bolm (Eds.), Transition Metals for Organic Synthesis, second ed., vol. 2, Wiley–VCH, Weinheim/New York, 2004, pp. 215–242 (Chapter 2.2).
[33] G.B. Shul'pin, E.R. Lachter, J. Mol. Cat. A 197 (2003) 65–71.
[34] M. Bühl, R. Schurhammer, P. Imhof, J. Am. Chem. Soc. 126 (2004) 3310–3320.
[35] T.K. Si, K. Chowdhury, M. Mukherjee, D.C. Bera, R. Bhattacharyya, J. Mol. Catal. A 219 (2004) 241–247.
[36] Y. Nakagawa, K. Kamata, M. Kotani, K. Yamaguchi, N. Mizuno, Angew. Chem. Int. Ed. 44 (2005) 5136–5141.
[37] A.P. Pokutsa, J. Le Bras, J. Muzart, Izv. Akad. Nauk., Ser. Khim. (2005) 307–310 (in Russian).
[38] P.M. Reis, J.A.L. Silva, A.F. Palavra, J.J.R. Fraústo da Silva, A.J.L. Pombeiro, J. Catal. 235 (2005) 333–340.
[39] S. Shinachi, M. Matsushita, K. Yamaguchi, N. Mizuno, J. Catal. 233 (2005) 81–89.
[40] X. Gao, J. Xu, Catal. Lett. 111 (2006) 203–205.
[41] V.N. Shetti, M.J. Rani, D. Srinivas, P. Ratnasamy, J. Phys. Chem. B 110 (2006) 677–679.
[42] L. Chen, B. Yang, X. Zhang, W. Dong, K. Cao, X. Zhang, Energy Fuels 20 (2006) 915–918.
[43] N. Mizuno, Y. Nakagawa, K. Yamaguchi, J. Mol. Catal. A 251 (2006) 286–290.
[44] M. Jian, L. Zhu, J. Wang, J. Zhang, G. Li, C. Hu, J. Mol. Catal. A 253 (2006) 1–7.
[45] S. Jing, Z. Wang, W. Zhu, J. Guan, G. Wang, React. Kinet. Catal. Lett. 89 (2006) 55–61.
[46] A.J.L. Pombeiro, ACS Symposium Series 974 (2007) 51–60.
[47] C.-H. Lee, T.-S. Lin, C.-Y. Mou, J. Phys. Chem. C 111 (2007) 3873–3882.
[48] D. Maity, J. Marek, W.S. Sheldrick, H. Mayer-Figge, M. Ali, J. Mol. Catal. A 270 (2007) 153–159.
[49] M.V. Kirillova, J.A.L. da Silva, J.J.R. Fraústo da Silva, A.J.L. Pombeiro, Appl. Catal. A 332 (2007) 159–165.
[50] M.V. Kirillova, M.L. Kuznetsov, P.M. Reis, J.A.L. da Silva, J.J.R. Fraústo da Silva, A.J.L. Pombeiro, J. Am. Chem. Soc. 129 (2007) 10531–10545.
[51] M.V. Kirillova, A.M. Kirillov, P.M. Reis, J.A.L. Silva, J.J.R. Fraústo da Silva, A.J.L. Pombeiro, J. Catal. 248 (2007) 130–136.
[52] M.V. Kirillova, J.A.L. da Silva, J.J.R. Fraústo da Silva, A.F. Palavra, A.J.L. Pombeiro, Adv. Synth. Catal. 349 (2007) 1765–1774.
[53] H. Ge, Y. Leng, C. Zhou, J. Wang, Catal. Lett. 124 (2008) 324–329.
[54] S. Tangestaninejad, V. Mirkhani, M. Moghadam, I. Mohammadpoor-Baltork, E. Shams, H. Salavati, Ultrasonics Sonochem. 15 (2008) 438–447.
[55] R. Sen, R. Bera, A. Bhattacharjee, P. Gütlich, S. Ghosh, A.K. Mukherjee, S. Koner, Langmuir 24 (2008) 5970–5975.
[56] M.V. Kirillova, M.L. Kuznetsov, J.A.L. da Silva, M.F.C.G. da Silva, J.J.R. Fraústo da Silva, A.J.L. Pombeiro, Chem. Eur. J. 14 (2008) 1828–1842.
[57] T.F.S. Silva, E.C.B.A. Alegria, L.M.D.R.S. Martins, A.J.L. Pombeiro, Adv. Synth. Catal. 350 (2008) 706–716.
[58] J. Arichi, M. Eternot, B. Louis, Catal. Today 138 (2008) 117–122.
[59] J. Zhao, W. Wang, Y. Zhang, J. Inorg. Organometal. Polym. Mater. 18 (2008) 441–447.

[60] Y.F. Lü, L.Z. Zhu, Q.Y. Liu, B. Guo, X.K. Hu, C.W. Hu, Chinese Chem. Lett. 20 (2009) 238–240.
[61] J.K. Joseph, S. Singhal, S.L. Jain, R. Sivakumaran, B. Kumar, B. Sain, Catal. Today 141 (2009) 211–214.
[62] E.F. Aboelfetoh, R. Pietschnig, Catal. Lett. 127 (2009) 83–94.
[63] G.B. Shul'pin, Mini-Rev. Org. Chem. (Bentham) 6 (2009) 95–104.
[64] G.B. Shul'pin, D. Attanasio, L. Suber, Russ. Chem. Bull. 42 (1993) 55–59.
[65] G.B. Shul'pin, A.N. Druzhinina, G.V. Nizova, Russ. Chem. Bull. 42 (1993) 1327–1329.
[66] G.V. Nizova, G.B. Shul'pin, Russ. Chem. Bull. 43 (1994) 1146–1148.
[67] G.B. Shul'pin, G. Süss- Fink, J. Chem. Soc., Perkin Trans. 2 (1995) 1459–1463.
[68] G.B. Shul'pin, R.S. Drago, M. Gonzalez, Russ. Chem. Bull. 45 (1996) 2386–2388.
[69] M.C. Guerreiro, U. Schuchardt, G.B. Shul'pin, Russ. Chem. Bull. 46 (1997) 749–754.
[70] G.B. Shul'pin, M.C. Guerreiro, U. Schuchardt, Tetrahedron 52 (1996) 13051–13062.
[71] G.V. Nizova, G. Süss-Fink, G.B. Shul'pin, Tetrahedron 53 (1997) 3603–3614.
[72] U. Schuchardt, M.C. Guerreiro, G.B. Shul'pin, Russ. Chem. Bull. 47 (1998) 247–252.
[73] G. Süss-Fink, G.V. Nizova, S. Stanislas, G.B. Shul'pin, J. Mol. Catal. A 130 (1998) 163–170.
[74] G.B. Shul'pin, Y. Ishii, S. Sakaguchi, T. Iwahama, Russ. Chem. Bull. 48 (1999) 887–890.
[75] G.B. Shul'pin, Y.N. Kozlov, G.V. Nizova, G. Süss-Fink, S. Stanislas, A. Kitaygorodskiy, V.S. Kulikova, J. Chem. Soc., Perkin Trans. 2 (2001) 1351–1371.
[76] M.H.C. de la Cruz, Y.N. Kozlov, E.R. Lachter, G.B. Shul'pin, New J. Chem. 27 (2003) 634–638.
[77] Y.N. Kozlov, G.V. Nizova, G.B. Shul'pin, J. Mol. Catal. A 227 (2005) 247–253.
[78] M.J.D.M. Jannini, L.S. Shul'pina, U. Schuchardt, G.B. Shul'pin, Petrol. Chem. 45 (2005) 413–418.
[79] Y.N. Kozlov, V.B. Romakh, A. Kitaygorodskiy, P. Buglyó, G. Süss-Fink, G.B. Shul'pin, J. Phys. Chem. A 111 (2007) 7736–7752.
[80] G.B. Shul'pin, D. Attanasio, L. Suber, J. Catal. 142 (1993) 147–152.
[81] G.V. Nizova, G. Süss-Fink, G.B. Shul'pin, Chem. Commun. (1997) 397–398.
[82] G. Süss-Fink, H. Yan, G.V. Nizova, S. Stanislas, G.B. Shul'pin, Russ. Chem. Bull. 46 (1997) 1801–1803.
[83] G.V. Nizova, G. Süss-Fink, S. Stanislas, G.B. Shul'pin, Chem. Commun. (1998) 1885–1886.
[84] G. Süss-Fink, S. Stanislas, G.B. Shul'pin, G.V. Nizova, H. Stoeckli-Evans, A. Neels, C. Bobillier, S. Claude, J. Chem. Soc., Dalton Trans. (1999) 3169–3175.
[85] G. Süss-Fink, S. Stanislas, G.B. Shul'pin, G.V. Nizova, Appl. Organometal. Chem. 14 (2000) 623–628.
[86] Y.N. Kozlov, G.V. Nizova, G.B. Shul'pin, Russ. J. Phys. Chem. 75 (2001) 770–774.
[87] G.B. Shul'pin, Y.N. Kozlov, Org. Biomol. Chem. 1 (2003) 2303–2306.
[88] G.V. Nizova, Y.N. Kozlov, G.B. Shul'pin, Russ. Chem. Bull. (2004) 2330–2333.
[89] G. Süss-Fink, L. Gonzalez Cuervo, B. Therrien, H. Stoeckli-Evans, G.B. Shul'pin, Inorg. Chim. Acta 357 (2004) 475–484.
[90] G.B. Shul'pin, G.S. Mishra, L.S. Shul'pina, T.V. Strelkova, A.J.L. Pombeiro, Catal. Commun. 8 (2007) 1516–1520.
[91] V.B. Romakh, G. Süss-Fink, G.B. Shul'pin, Petrol. Chem. 48 (2008) 440–443.
[92] L.S. Shul'pina, M.V. Kirillova, A.J.L. Pombeiro, G.B. Shul'pin, Tetrahedron 65 (2009) 2424–2429.
[93] G.V. Nizova, B. Krebs, G. Süss-Fink, S. Schindler, L. Westerheide, L. Gonzalez Cuervo, G.B. Shul'pin, Tetrahedron 58 (2002) 9231–9237.
[94] G.B. Shul'pin, G.V. Nizova, Y.N. Kozlov, L. Gonzalez Cuervo, G. Süss-Fink, Adv. Synth. Catal. 346 (2004) 317–332.
[95] V.B. Romakh, B. Therrien, G. Süss-Fink, G.B. Shul'pin, Inorg. Chem. 46 (2007) 3166–3175.
[96] S. Tanase, P. Marques-Gallego, W.R. Browne, R. Hage, E. Bouwman, B.L. Feringa, J. Reedijk, Dalton Trans. (2008) 2026–2033.
[97] U. Schuchardt, D. Mandelli, G.B. Shul'pin, Tetrahedron Lett. 37 (1996) 6487–6490.
[98] H.Q.N. Gunaratne, M.A. McKervey, S. Feutren, J. Finlay, J. Boyd, Tetrahedron Lett. 39 (1998) 5655–5658.
[99] R. Saladino, P. Carlucci, M.C. Danti, C. Crestini, E. Mincione, Tetrahedron 56 (2000) 10031–10037.
[100] G.V. Nizova, G.B. Shul'pin, Tetrahedron 63 (2007) 7997–8001.
[101] R.Z. Khaliullin, A.T. Bell, M. Head-Gordon, J. Phys. Chem. B 109 (2005) 17984–17992.
[102] M.L. Kuznetsov, A.J.L. Pombeiro, Inorg. Chem. 48 (2009) 307–318.
[103] M.G. Voronkov, O.A. Osipov, V.A. Kogan, V.A. Chetverikov, A.F. Lapsin, Khim. Geterotsikl. Soedin. (1967) 35–38 (in Russian).
[104] D.C. Crans, H. Chen, O.P. Anderson, M.M. Miller, J. Am. Chem. Soc. 115 (1993) 6769–6776.
[105] W.A. Nugent, R.L. Harlow, J. Am. Chem. Soc. 116 (1994) 6142–6148.
[106] G. Wagner, R. Herrmann, A.J.L. Pombeiro, Inorg. Chim. Acta 336 (2002) 147–150.
[107] P.M. Reis, J.A.L. Silva, J.J.R. Fraústo da Silva, A.J.L. Pombeiro, J. Mol. Catal. A 224 (2004) 189–195.
[108] A.D. Becke, J. Chem. Phys. 98 (1993) 5648–5652.
[109] C. Lee, W. Yang, R.G. Parr, Phys. Rev. B 37 (1988) 785–789.
[110] M.J. Frisch, G.W. Trucks, H.B. Schlegel, G.E. Scuseria, M.A. Robb, J.R. Cheeseman, V.G. Zakrzewski , J.A. Montgomery Jr., R.E. Stratmann, J.C. Burant, S. Dapprich, J.M. Millam, A.D. Daniels, K.N. Kudin, M.C. Strain, O. Farkas, J. Tomasi, V. Barone, M. Cossi, R. Cammi, B. Mennucci, C. Pomelli, C. Adamo, S. Clifford, J. Ochterski, G.A. Peterson, P.Y. Ayala, Q. Cui, K. Morokuma, D.K. Malick, A.D. Rabuck, K. Raghavachari, J.B. Foresman, J. Cioslowski, J.V. Ortiz, A.G. Baboul, B.B. Stefanov, G. Liu, A. Liashenko, P. Piskorz, I. Komaromi, R. Gomperts, R.L. Martin, D.J. Fox, T. Keith, M.A. Al-Laham, C.Y. Peng, A. Nanayakkara, M. Challacombe, P.M.W. Gill, B. Johnson, W. Chen, M.W. Wong, J.L. Andres, C. Gonzalez, M. Head-Gordon, E.S. Replogle, J.A. Pople, Gaussian 98, Revision A.9, Gaussian, Inc. Pittsburgh, PA, 1998.
[111] M. Dolg, U. Wedig, H. Stoll, H. Preuss, J. Chem. Phys. 86 (1987) 866–872.
[112] J. Tomasi, M. Persico, Chem. Rev. 94 (1997) 2027–2094.
[113] V. Barone, M. Cossi, J. Phys. Chem. 102 (1998) 1995–2001.
[114] M.J. Frisch, G.W. Trucks, H.B. Schlegel, G.E. Scuseria, M.A. Robb, J.R. Cheeseman, J.A. Montgomery Jr., T. Vreven, K.N. Kudin, J.C. Burant, J.M. Millam, S.S. Iyengar, J. Tomasi, V. Barone, B. Mennucci, M. Cossi, G. Scalmani, N. Rega, G.A. Petersson, H. Nakatsuji, M. Hada, M. Ehara, K. Toyota, R. Fukuda, J. Hasegawa, M. Ishida, T. Nakajima, Y. Honda, O. Kitao, H. Nakai, M. Klene, X. Li, J.E. Knox, H.P. Hratchian, J.B. Bakken, V. Cross, C. Adamo, J. Jaramillo, R. Gomperts, R.E. Stratmann, O. Yazyev, A.J. Austin, R. Cammi, C. Pomelli, J.W. Ochterski, P.Y. Ayala, K. Morokuma, G.A. Voth, P. Salvador, J.J. Dannenberg, V.G. Zakrzewski, S. Dapprich, A.D. Daniels, M.C. Strain, O. Farkas, D.K. Malick, A.D. Rabuck, K. Raghavachari, J.B. Foresman, J.V. Ortiz, Q. Cui, A.G. Baboul, S. Clifford, J. Cioslowski, B.B. Stefanov, G. Liu, A. Liashenko, P. Piskorz, I. Komaromi, R.L. Martin, D.J. Fox, T. Keith, M.A. Al-Laham, C.Y. Peng, A. Nanayakkara, M. Challacombe, P.M.W. Gill, B. Johnson, W. Chen, M.W. Wong, C. Gonzalez, J.A. Pople, Gaussian 03, Revision D.01; Gaussian, Inc., Wallingford, CT, 2004.
[115] G.H. Wertz, J. Am. Chem. Soc. 102 (1980) 5316–5322.
[116] J. Cooper, T. Ziegler, Inorg. Chem. 41 (2002) 6614–6622.
[117] D.Z. Rehder, Naturforsch. B: Chem. Sci. 32 (1977) 771–775.
[118] K. Paulsen, D.Z. Rehder, Naturforsch. A: Phys. Sci. 37 (1982) 139–149.
[119] W. Priebsch, D. Rehder, Inorg. Chem. 24 (1985) 3058–3062.
[120] M. Bonchio, O. Bortolini, M. Carraro, V. Conte, S. Primon, J. Inorg. Biochem. 80 (2000) 191–194.
[121] V. Conte, F. Di Furia, S. Moro, J. Mol. Catal. A 117 (1997) 139–149.
[122] V. Conte, F. Di Furia, S. Moro, J. Mol. Catal. A 94 (1994) 323–333.
[123] J.A. Riddick, W.B. Bunger, T.K. Sakano, Organic Solvents: Physical Properties and Methods of Purification, fourth ed., Wiley-Interscience, New York, 1986.
[124] G.B. Shul'pin, J. Chem. Res. (S) (2002) 351–353.
[125] G.B. Shul'pin, A.R. Kudinov, L.S. Shul'pina, E.A. Petrovskaya, J. Organomet. Chem. 691 (2006) 837–845.
[126] G.B. Shul'pin, G. Süss-Fink, A.E. Shilov, Tetrahedron Lett. 42 (2001) 7253–7256.
[127] V.A. dos Santos, L.S. Shul'pina, D. Veghini, D. Mandelli, G.B. Shul'pin, React. Kinet. Catal. Lett. 88 (2006) 339–348.
[128] V.B. Romakh, B. Therrien, G. Süss-Fink, G.B. Shul'pin, Inorg. Chem. 46 (2007) 1315–1331.
[129] G.B. Shul'pin, M.G. Matthes, V.B. Romakh, M.I.F. Barbosa, J.L.T. Aoyagi, D. Mandelli, Tetrahedron 64 (2008) 2143–2152.
[130] G.B. Shul'pin, Y.N. Kozlov, S.N. Kholuiskaya, M.I. Plieva, J. Mol. Catal. A 299 (2009) 77–87.
[131] G. Zampella, P. Fantucci, V.L. Pecoraro, L. De Gioia, Inorg. Chem. 45 (2006) 7133–7143.
[132] M.L. Kuznetsov, A.A. Nazarov, L.V. Kozlova, V.Y. Kukushkin, J. Org. Chem. 72 (2007) 4475–4485.
[133] M.L. Kuznetsov, V.Y. Kukushkin, J. Org. Chem. 71 (2006) 582–592.
[134] M.L. Kuznetsov, V.Y. Kukushkin, A.I. Dement'ev, A.J. L Pombeiro, J. Phys. Chem. A 107 (2003) 6108–6120.